Click Here for Full Article

Pacific Plate subduction beneath the central Mariana and Izu-Bonin fore arcs: New insights from an old margin

A. J. Oakley, B. Taylor, and G. F. Moore

Department of Geology and Geophysics, SOEST, University of Hawaii at Manoa, 1680 East West Road, Honolulu, Hawaii 96822, USA (aoakley@hawaii.edu; taylorb@hawaii.edu; gmoore@hawaii.edu)

[1] Multichannel seismic (MCS) profiles and bathymetric data from the central Mariana and Izu-Bonin subduction systems image the subducting Pacific Plate from the outer trench slope to beneath serpentinite seamounts on the outer fore arc. Subducting oceanic crust varies along the Mariana margin from 5.3 to 7 km thick and is covered by 0.5–2 km thick sediments and numerous seamounts. Oceanic crustal thickness east of the Izu-Bonin Trench is ~6 km. Faulting resulting from flexure of the incoming Pacific Plate begins up to 100 km east of the trench axis, near the 6 km depth contour. The plate is cut by normal faults that reactivate inherited tectonic fabric where that fabric strikes $<25°$ to the trench. Where the strike is $>25°$, incoming crust breaks along new faults with a trench-parallel strike. The Mariana Trench axis is commonly a graben that accommodates an abrupt change (within <25 km) of plate dip from $<4°$ (commonly $\leq 2°$) on the incoming plate to $>8°$ beneath the outer fore arc. We infer that the plate fails there rather than simply bends under the applied loads. Along portions of the Mariana margin, subducting seamounts displace the trench axis westward and uplift the toe of the slope. Surprisingly, west of the toe, there is no geophysical evidence of disturbance of the upper plate in response to seamount subduction, nor of significant subduction erosion or sediment underplating. MCS profiles across the base of the Mariana inner trench slope provide evidence for both complete subduction and small-scale accretion of Pacific Plate sediments; however, we found no evidence for long-term sediment accretion. The subducting plate dips 9–12° beneath serpentinite seamounts on the Izu-Bonin and Mariana fore arcs. Along the Mariana margin, the majority of these seamounts are located ~50–70 km west of the trench where the mantle wedge is 3–7 km thick between 8–10 km thick fore-arc crust and the top of the subducting plate. The apparent lack of significant deformation of the Mariana fore arc crust by subducting seamounts may be the result of a weak serpentinized mantle wedge and/or progressive fracturing as the subducting plate increases in dip as it passes through the trench graben.

1. Introduction

[2] Subduction zones recycle near-surface materials (sediments, fluids, crust and depleted mantle lithosphere) to beneath the zone of arc and back-arc magma genesis and thence deeper into the asthenosphere. From the trench outer rise to the deep subducted slab, the inputs to the subduction zone are deformed, added to, and subtracted from, resulting in diverse surficial products and mantle modifications, earthquake seismicity patterns and slab geometries. Arc volcanism carries the signatures of subducted sediments, fluids, and crust to varying degrees, raising questions as to what processes are responsible for the variability [e.g., *Plank and Langmuir*, 1993; *Elliott et al.*, 1997].

[3] Normal faulting that accompanies flexural bending of the incoming plate into the trench [*Bodine and Watts*, 1979] may facilitate the addition of fluid to the subduction system [*Ranero and Sallares*, 2004]. For example, *Ranero et al.* [2003] propose that normal faults along the Middle-America Trench cut >20 km into the subducting plate and serve as pathways for fluids to serpentinize the subducting plate mantle. The subduction of seamounts may locally uplift and tectonically erode the toe of the overriding plate, which collapses as the seamount passes under the slope [e.g., *Lallemand et al.*, 1989; *Dominguez et al.*, 1998]. Sediments may be scraped off the downgoing plate to form accretionary prisms, underplated beneath the fore arc, and/or subducted to the depths of magma generation and beyond [*von Huene and Scholl*, 1991]. Relating the subduction inputs to volcanic outputs is simplified in non-accretionary intraoceanic subduction zones where the sedimentary section is assumed to be subducted completely and where there is no continental influence on sedimentation or magmatism. The Izu-Bonin-Mariana (IBM) arc – trench – back arc is the classic example of an intraoceanic subduction system [*Karig*, 1971a, 1971b; *Forsyth and Uyeda*, 1975; *Uyeda*, 1982; *Ricard et al.*, 1988] and the history of subduction input, volcanic output and back-arc spreading are well studied.

[4] *von Huene and Scholl* [1991] showed that sediment supply controls the balance between accretion and nonaccretion along subduction zones. On a global scale, regions with incoming sediments thicker than 1 km commonly have accretionary wedges, whereas areas with thinner incoming sediments are generally non-accretionary and may be erosional [*Clift and Vannucchi*, 2004].

The Mariana region has been cited as a type location for subduction erosion along a convergent margin [*Hussong and Uyeda*, 1981b], although this hypothesis is controversial [*Karig and Ranken*, 1983]. In regions without large accretionary prisms, small-scale offscraping and/or underplating of sediments may reduce the amount of sediment and fluid delivered to the subduction factory, and erosion of the fore arc in the wake of subducting seamounts may add material to the downgoing plate. Therefore an analysis of processes occurring within the trench and at the toe of the slope is essential to understand and quantify subduction inputs.

[5] Only a portion of the fluids that enter the subduction system bound in pore spaces and hydrous minerals in the subducting lithosphere will escape beneath the fore arc. Some fluid will descend to depths suitable for arc magma formation, while a small amount will subduct into the deep mantle [*Schmidt and Poli*, 1998]. *Peacock* [1990] calculates that most pore fluids are expelled at depths <10–40 km, and *Schmidt and Poli* [1998] predict that 30–70% of subducted water is released beneath the fore arc. The fluids migrating up from the subducting plate will cool and serpentinize the overriding fore-arc mantle [*Peacock*, 1990]. As evidence of these processes, serpentinite mud volcanoes erupt hydrated and comminuted mantle peridotite onto the Izu-Bonin-Mariana fore arc [*Fryer et al.*, 1985; *Oakley et al.*, 2007] (Figure 1). These mud volcanoes vent slab-derived fluids and represent some of the first outputs of the subduction system. The compaction and dehydration reactions that release fluid from the slab are depth-controlled, and therefore the fluid flux through the subduction zone is governed by the geometry of the subducting plate. This geometry is poorly constrained in most fore arcs because of the large depth uncertainties in the location of teleseismic earthquakes [*Engdahl et al.*, 1998]. With few local seismometer stations, seismicity data do not resolve the depth to the subducting plate beneath the serpentinite seamounts on the IBM fore arc.

[6] In this paper we present a detailed study of the central Mariana subduction zone and previously unpublished data from the Izu-Bonin region. Using multichannel seismic (MCS) reflection and swath bathymetry data, combined with the results of previous drilling, dredging and seismic surveys, we quantify subduction inputs, describe Pacific Plate flexure and propose that the plate fails, rather
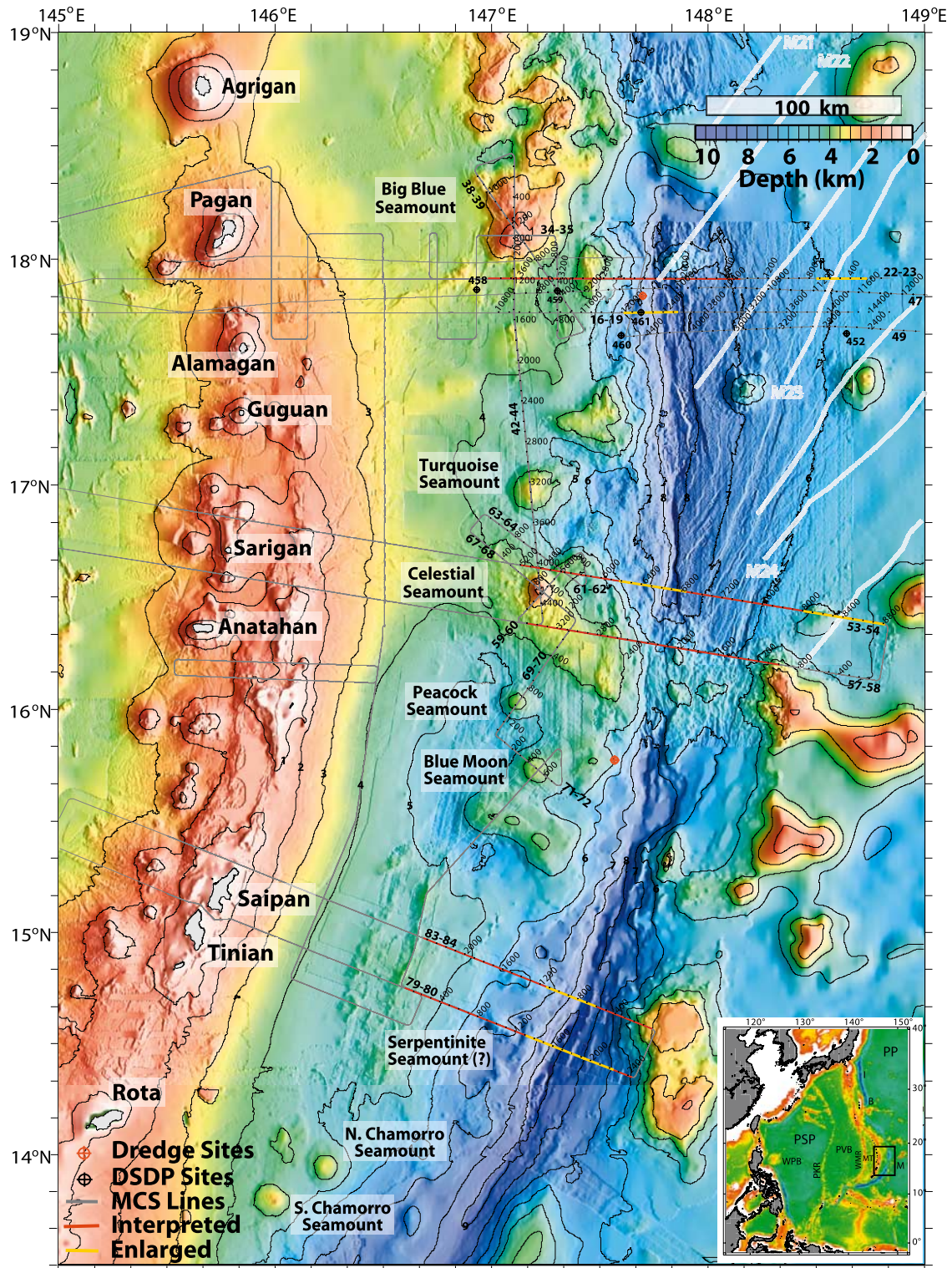
Figure 1. Regional location map. PSP, Philippine Sea Plate; PP, Pacific Plate; IBM, Izu-Bonin-Mariana Trenches; MT, Mariana Trough; WMR, West Mariana Ridge; PVB, Parece Vela Basin; PKR, Palau-Kushu Ridge; WPB, West Philippine Basin. Bathymetry of the central Mariana arc-trench system from combined surveys, sunlit from the east, showing EW0202 seismic lines. Interpreted lines are shown in red. Pacific Plate magnetic lineations from *Nakanishi et al.* [1992a] are drawn in white.

than simply bends, forming a trench axis graben. We show that the incoming sedimentary section is completely subducted in some regions of the central Mariana margin, but that small, ephemeral accretionary prisms occur in others. We find shallower dips and depths of the subducting plate beneath the outer fore arc than previously estimated, indicating a thinner mantle wedge beneath the serpentinite seamounts and much less release of subducted water. Unlike other margins, we are surprised to find little evidence for disturbance of the upper plate by subduction of large seamounts on the Pacific Plate.

[7] The standard view of the Mariana system comes from subduction cartoons that typify the margin at 18°N [e.g., *Hussong and Uyeda*, 1981a; *Eiler*, 2003], but this view is oversimplified and does not take into account variations along the margin. Here, we present variations along-strike of the Pacific Plate with implications for subduction factory inputs and plate flexure and create a new cross section of Pacific Plate subduction beneath the central Mariana fore arc. Our data reveal fundamental attributes of the Mariana subduction zone and enable improved comparisons with other intraoceanic margins such as Izu-Bonin and Tonga.

2. Geologic Setting and Previous Work

[8] Subduction began in the Izu-Bonin-Mariana convergent margin circa 50 Ma [*Taylor*, 1992; *Cosca et al.*, 1998]. Pacific Plate magnetic isochrons (M21–M25; 148–154 Ma) strike obliquely to the Mariana Trench (Figure 1) [*Nakanishi et al.*, 1992a]. Thinly sedimented (typically less than 500 m), Mesozoic Pacific Plate lithosphere subducts beneath the Mariana arc system [*LaTraille and Hussong*, 1980; *Hussong and Fryer*, 1981; *Nakanishi et al.*, 1992b]. The dip of the subducted Pacific Plate increases to near-vertical beneath the active volcanoes of the Mariana arc ~220 km from the Mariana Trench [*Katsumata and Sykes*, 1969; *Isacks and Barazangi*, 1977; *Chiu et al.*, 1991; *Engdahl et al.*, 1998], but details of the slab geometry beneath the fore arc are poorly resolved [*Engdahl et al.*, 1998].

[9] *Ewing et al.* [1968] characterized the seismic stratigraphy of the western Pacific using four units: (1) upper transparent layer, (2) upper opaque layer, (3) lower transparent layer, and (4) acoustic basement. Early Deep Sea Drilling Program (DSDP) drilling legs (e.g., 6, 7, 17, and 20) showed that the

upper opaque layer correlates with a layer of chert abundant in the North Pacific. Later drilling discovered a lower chert layer above, and sometimes in contact with, basement. In some regions, acoustic basement corresponds with this chert layer. Regional mapping of the stratigraphy of the Jurassic basins in the western Pacific [*Abrams et al.*, 1992] shows that pockets of thick sediments, usually volcaniclastics, are derived locally from seamounts on the Pacific Plate. Outside of these pockets, the incoming sediments are primarily <0.5 km thick and composed of clay, chert and volcaniclastic layers [*Abrams et al.*, 1992]. Ocean Drilling Program (ODP) Hole 801C drilled in the Pigafetta Basin at ~18°38.5′N, 156°21.6′E, sampled ~170 Ma normal mid-ocean-ridge basalt crust formed at a fast (160 mm/a) spreading center, comparable with the modern East Pacific Rise. Twenty meters of red radiolarites and claystones overlie basement at 461.6 mbsf [*Abrams et al.*, 1993]. The sedimentary section at Hole 801C is characterized by two chert layers (lower and upper) separated by a thick (192 m) deposit of mid-Cretaceous volcaniclastic turbidites likely shed from the Magellan Seamount chain. The thinner (63 m) upper layer (upper opaque) is composed of chert-porcelainite and is overlain by 56 m of pelagic clay (upper transparent).

[10] At ODP Site 1149 (31°20′N, 143°21′E), along the Izu-Bonin Trench (Figure 1 inset), the subducting sediment section lacks the thick volcaniclastic sequence sampled to the south and includes an upper layer of ash and siliceous clay [*Shipboard Scientific Party*, 2000]. The Pacific Plate crust subducting into the Izu-Bonin Trench is ~132 Ma and was formed at spreading rates of 51 mm/a [*Shipboard Scientific Party*, 2000]. Bending along the Izu-Bonin Trench is associated with large-offset horsts and graben that do not occur along the Mariana Trench to the south [*Bodine and Watts*, 1979]. West of the outer rise and north of the Ogasawara Plateau, the seafloor entering the Izu-Bonin Trench has few seamounts [*Wessel*, 2001].

[11] East of the Mariana Trench, the subducting Pacific Plate is dotted with seamounts 2–3 km high [*Wessel*, 2001] (Figure 1). Subduction of bathymetric highs on the incoming plate locally uplifts the toe of the overriding plate and can cause oversteepening and erosion, resulting in the creation of a reentrant and shallowing of the trench floor [*Lonsdale*, 1986; *Lallemand and Le Pichon*, 1987; *Lallemand et al.*, 1989, 1994; *von Huene*
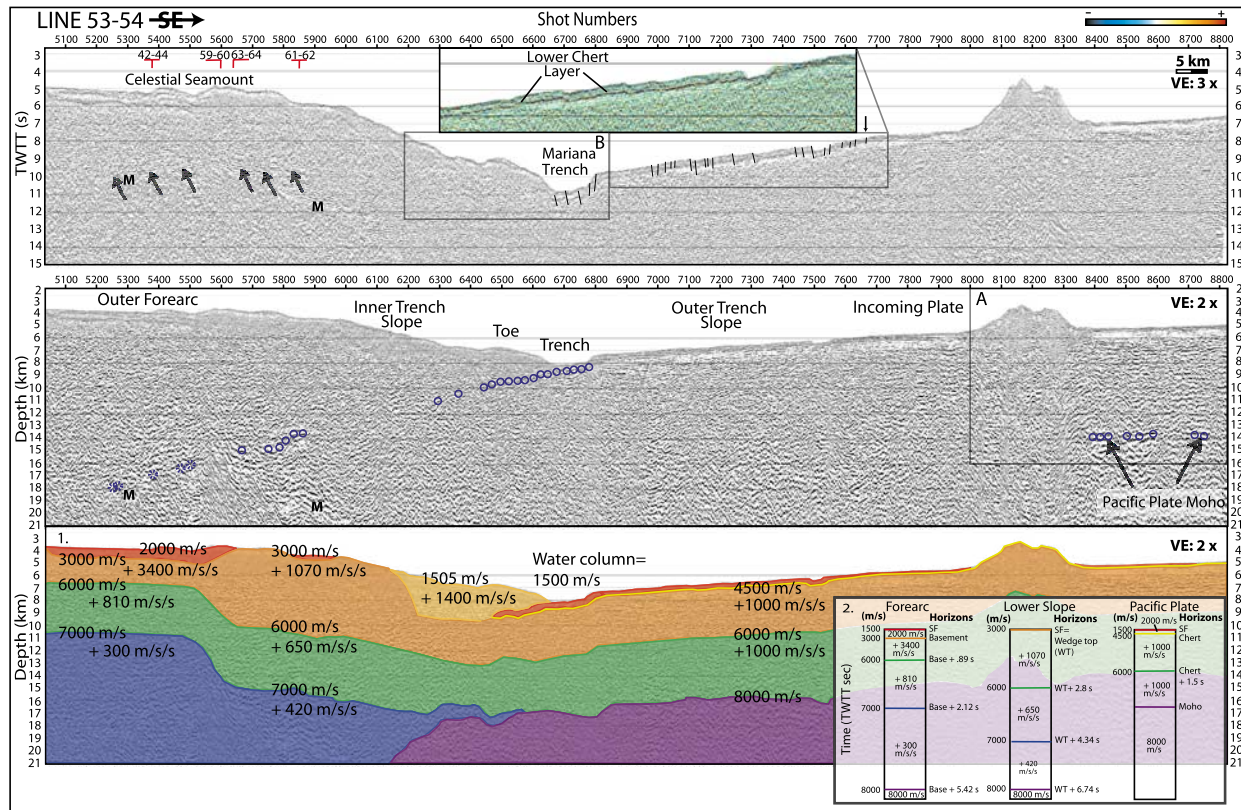
Figure 2. Time and depth sections of MCS Line 53–54. Location on Figure 1. TWTT, two-way travel time; M, seafloor multiple. A black arrow marks the beginning of bending-related faulting on the incoming Pacific Plate. Hollow circles on the incoming plate indicate Pacific Plate Moho. The prominent, low-frequency reflection beneath the outer fore arc is interpreted to be the top of the subducting plate (indicated by hollow arrows on the time section). Circles locate the points along the plate reflection where depths were recorded (visible in map view on Figure 3). Dashed circles represent B-picks. This profile is representative of the Pacific Plate entering the Mariana Trench in Region B. Boxes A and B refer to the areas enlarged in Figures 10 and 11a. (1) Velocity model overlain in depth on Line 53–54 based on the refraction line from *Takahashi et al.* [2007] and Pacific Plate drill sites. (2) Schematic vertical columns in time showing horizons, velocities (m/s), and gradients (m/s/s) used for the depth conversions of all MCS lines. The lower slope column represents a low-velocity region near the serpentinite seamounts. Where there were no seamounts present, only the Forearc and Pacific Plate velocity columns were used.

and Scholl, 1991]. The effect of seamount subduction is well documented along other margins including the Japan Trench, Tonga and Costa Rica [e.g., *Lallemand and Le Pichon*, 1987; *Ballance et al.*, 1989; *Lallemand et al.*, 1989; *Yamazaki and Okamura*, 1989; *Ranero and von Huene*, 2000], and previous work states that subducting oceanic plateaus and seamounts have uplifted the Mariana fore arc, creating and re-activating faults [*Fryer and Fryer*, 1987; *Fryer et al.*, 1995, 2000]. Sandbox models and geophysical observations suggest that the subduction of bathymetric highs (ridges and seamounts) is responsible for an important part of tectonic erosion along the inner trench slope [e.g., *Ballance et al.*, 1989; *Yamazaki and Okamura*, 1989; *Dominguez et al.*, 2000].

[12] Drilling, dredging and seismic imaging reveal that the outer Mariana fore arc does not have a substantial sedimentary cover or accretionary prism, but primarily exposes middle-upper Eocene igneous basement composed of arc tholeiites and boninites [*Hussong and Uyeda*, 1981b; *Mrozowski et al.*, 1981; *Bloomer*, 1983]. The presence of igneous rocks of island arc affinity on the inner trench slope is one reason why Mariana has been classified as an erosional margin [*Bloomer and Hawkins*, 1983].

[13] Serpentinite seamounts occur ~30 to 100 km west of the IBM Trench axis [*Fryer and Hussong*, 1981; *Fryer and Fryer*, 1987; *Horine et al.*, 1990; *Fryer and Mottl*, 1992] and retain some blueschist minerals originating at depths >20 km [*Maekawa*
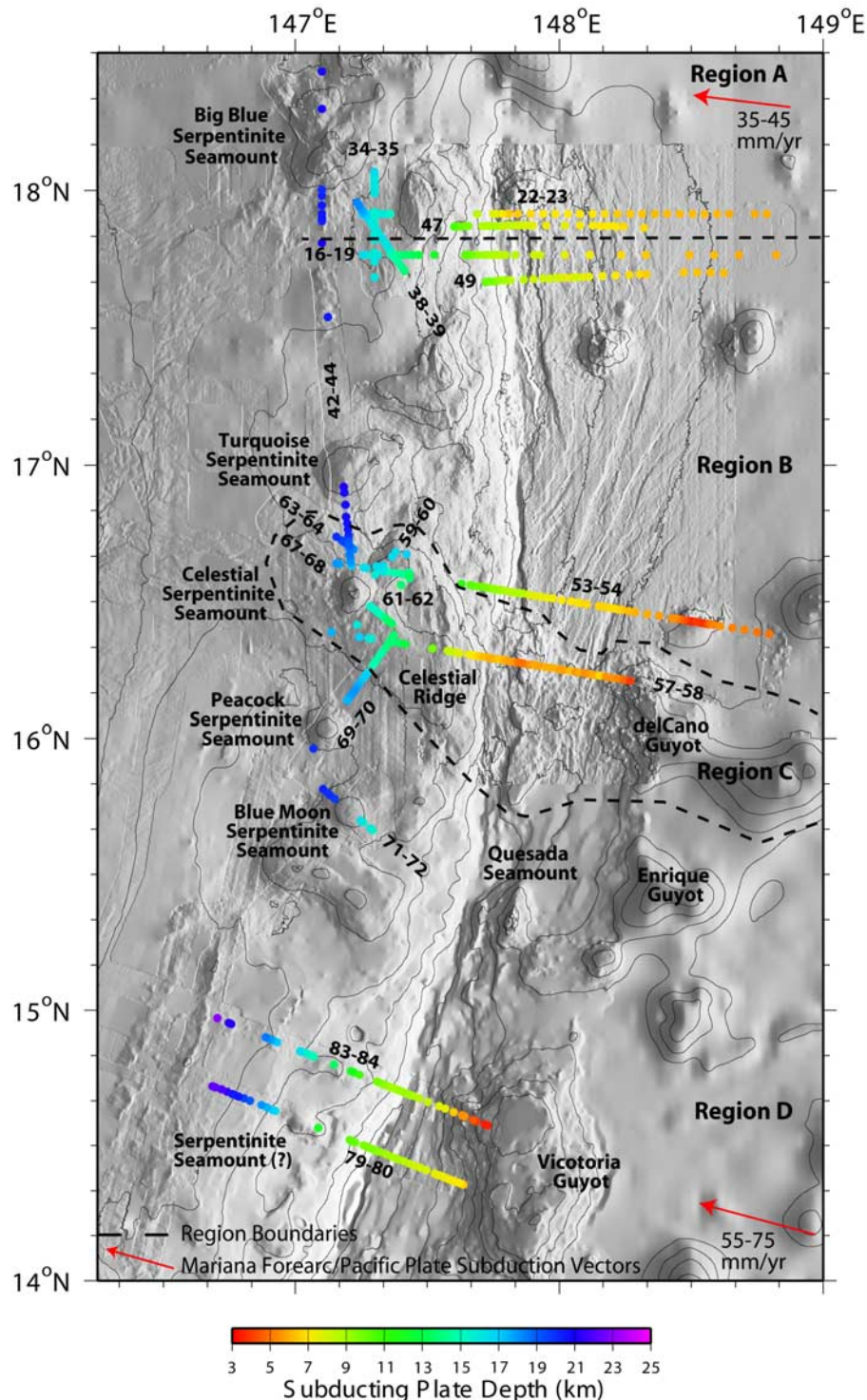
Figure 3. Highlighted Mariana fore-arc bathymetry showing the location and depths of all picks along the subducting Pacific Plate chert layer and top of plate reflection from 17 MCS reflection profiles. The serpentinite seamounts on the outer fore arc and named seamounts on the Pacific Plate are labeled.

et al., 1995; Gharib, 2006]. Active carbonate and Mg-silicate chimneys and cold-fluid seeps at the summits of many serpentinite seamounts provide samples of the chemical precipitates and fluids that

result from initial slab de-volatilization [Fryer et al., 1985; Haggerty, 1987; Mottl, 1992; Mottl et al., 2003; Straub and Layne, 2003]. The chemistry of these vent fluids varies systematically with
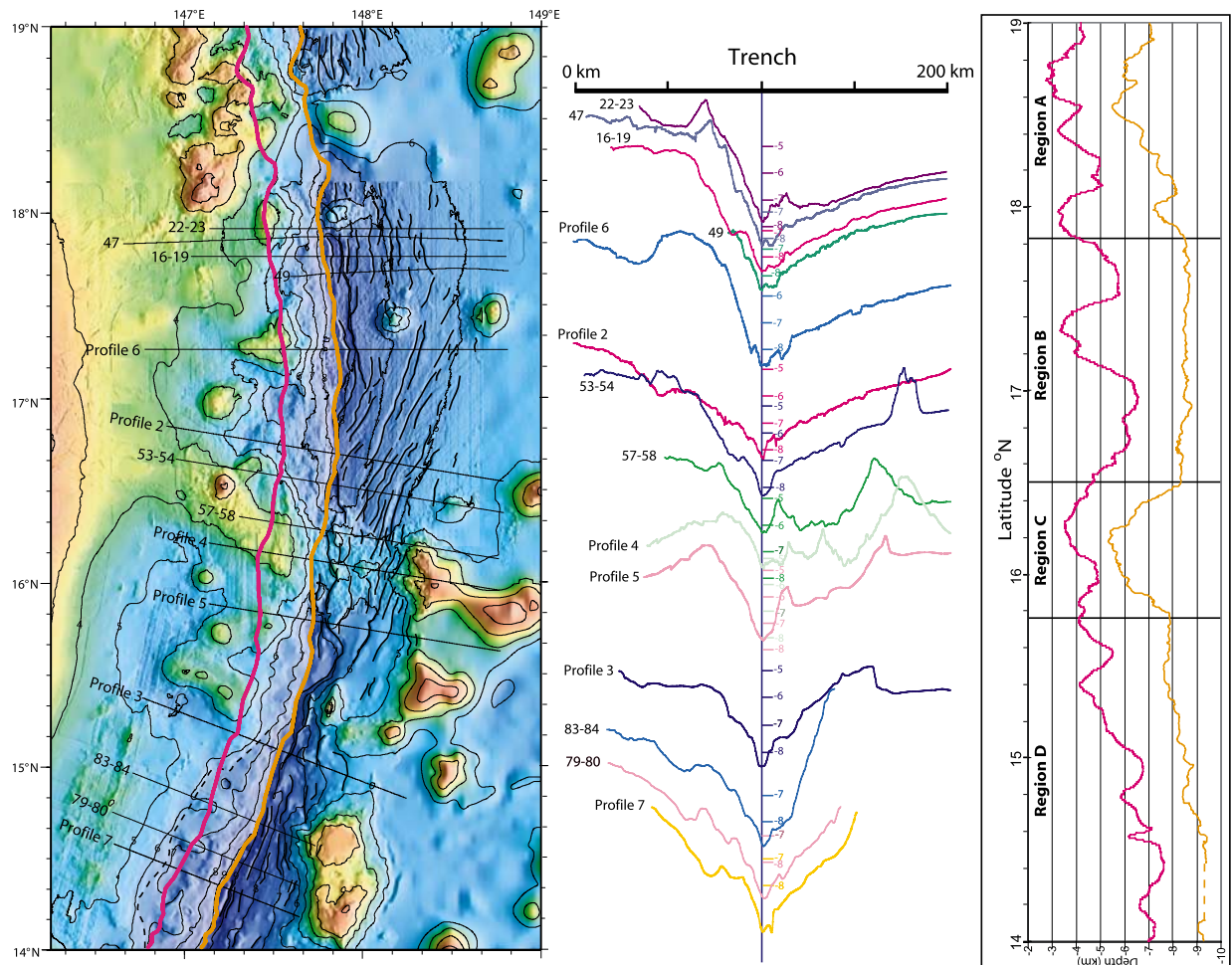
Figure 4. Bathymetry along MCS tracks and generated profiles across the central Mariana Trench plotted from west to east. Flexure-related faults are outlined in black. The dashed line on the bathymetric map outlines the lower slope terrace in Region D. VE~14x. Depth versus latitude along the Central Mariana Trench axis (orange) and outer fore arc (pink). Vertical lines represent region boundaries shown on Figure 3.

distance from the trench, implying little mixing of fluids along the subduction interface [*Mottl et al.*, 2003, 2004]. These data support the current model for Mariana serpentinite mud volcano formation that suggests that there is serpentinized mantle directly beneath the edifice [*Fryer et al.*, 2000].

[14] The restriction of the serpentinite seamounts to a band of fore arc ~70 km wide may be related to slab dewatering processes, controlled by temperature and depth, and the location of the fore-arc mantle wedge. Because serpentine minerals are stable until depths greater than the region of magma generation in cold subduction zones like IBM [*Ulmer and Trommsdorff*, 1995; *Schmidt and Poli*, 1998; *Hyndman and Peacock*, 2003], the primary fluids liberated from the subducted plate beneath the Mariana fore arc are derived from

oceanic sediments and crust, rather than serpentinized mantle.

3. Data Acquisition and Processing

[15] We collected multichannel seismic (MCS) data from the central Mariana arc system in February–March, 2002 aboard the R/V *Maurice Ewing* towing a 6-km, 480-channel streamer cable. Shots were fired every 50 m from a tuned, 6817 inch³ array of 20 air guns. The processing sequence applied to all lines is listed in Table A1. In areas where water depths are less than 4 km, the plate reflection is obscured by the seafloor multiple necessitating the use of multiple suppression techniques.

[16] The seismic data are presented here in two-way travel time (TWTT) with a vertical exagger-
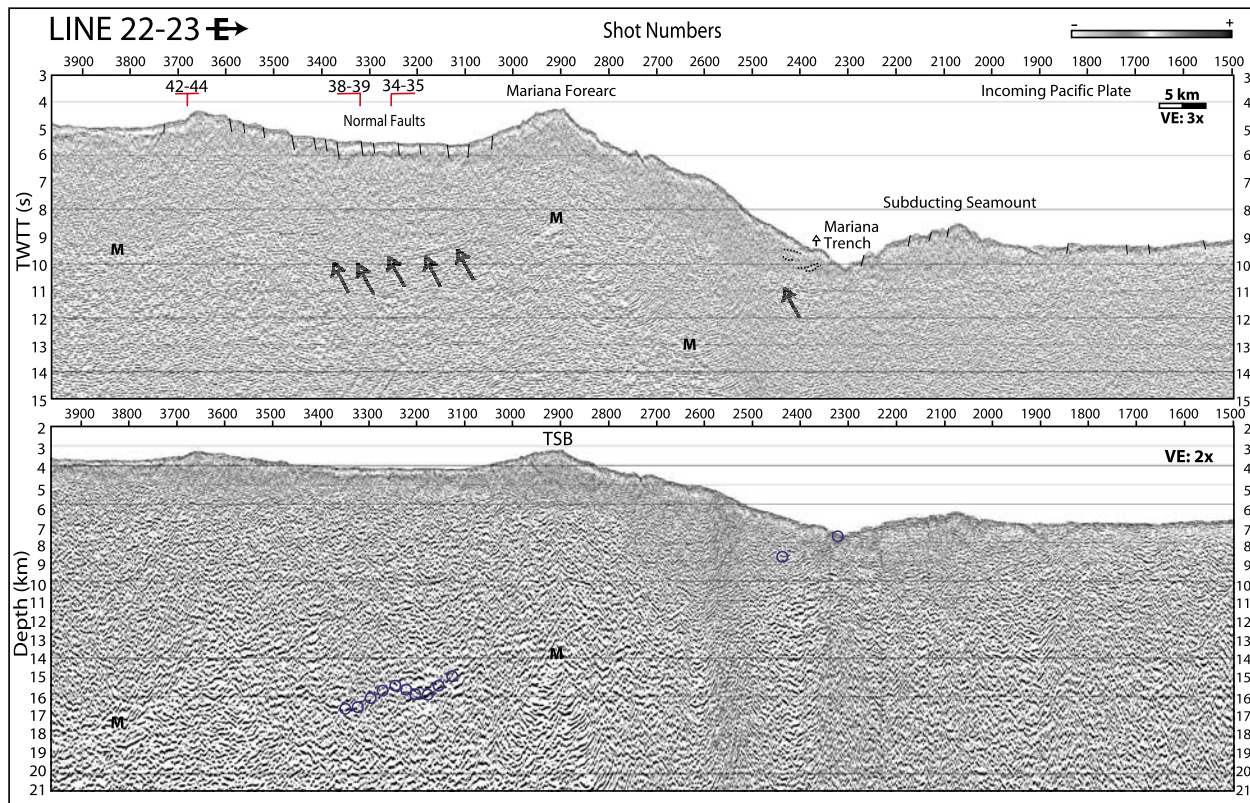
Figure 5. Time and depth sections of MCS Line 22–23. Symbols are the same as in Figure 2. This profile is representative of the Pacific Plate entering the Mariana Trench in Region A. Normal faults on the incoming plate and the Mariana fore arc are interpreted. The toe of the fore arc is uplifted as the flank of a Pacific Plate seamount subducts. TSB, trench slope break; M, seafloor multiple. Location on Figure 1.

ation (VE) of 3x at the seafloor, and in depth at VE = 2x. Our velocity models for depth conversion in the outer fore arc are based on a refraction survey across the Mariana fore arc that extends to the 6 km depth limit of the OBSs used [*Takahashi et al.*, 2007]. This refraction line is coincident with MCS Line 53–54, which trends ESE across the northern flank of Celestial Seamount (Figure 2). The velocity model of *Takahashi et al.* [2007] has a low-velocity wedge beneath the serpentinite seamount. The velocities of the subducting plate are not represented in the OBS crustal velocity model; therefore, we did not include incoming plate velocities beneath the outer fore arc in the depth conversion. Interval velocities for the incoming plate were based upon data from DSDP and ODP drill sites east of the trench (Sites 801 and 459). Our velocity model is overlain in depth on MCS Line 53–54 in Figure 2. In addition to the standard crustal/sediment velocities shown in Figure 2, we used a velocity of 1505 m/s (a slight increase from the water column velocity) plus a vertical gradient of 1400 m/s/s to depth convert material at the toe of the slope and serpentinite seamounts where pres-

ent. These values successfully correct for velocity pull up of the top of plate reflection near the base of the inner trench slope. The rationale for the velocities applied to the serpentinite seamounts is detailed in [*Oakley et al.*, 2007].

[17] MCS data from the Izu-Bonin margin collected aboard the R/V *Robert Conrad* in 1976 are processed through migration and presented in TWTT. Depths to the top of the subducting plate on Bonin Line 39 were determined using the refraction velocities of *Kamimura et al.* [2002].

[18] The Mariana bathymetric maps used in this study contain Hydrosweep data from the EW0202/03 cruises, Simrad EM300 data from a 2003 R/V *Thompson* cruise, 1997 HAWAII MR-1 data, and data from a composite of regional studies conducted on ships from the Japan Agency for Marine Earth Science and Technology (JAMSTEC) (N. Seama and M. Nakanishi, private communications, 2002). The Izu-Bonin bathymetry uses multibeam data provided by the second author, A. Klaus, A. Taira and K. Fujioka (JAMSTEC and Ocean Research Institute, University of Tokyo). The
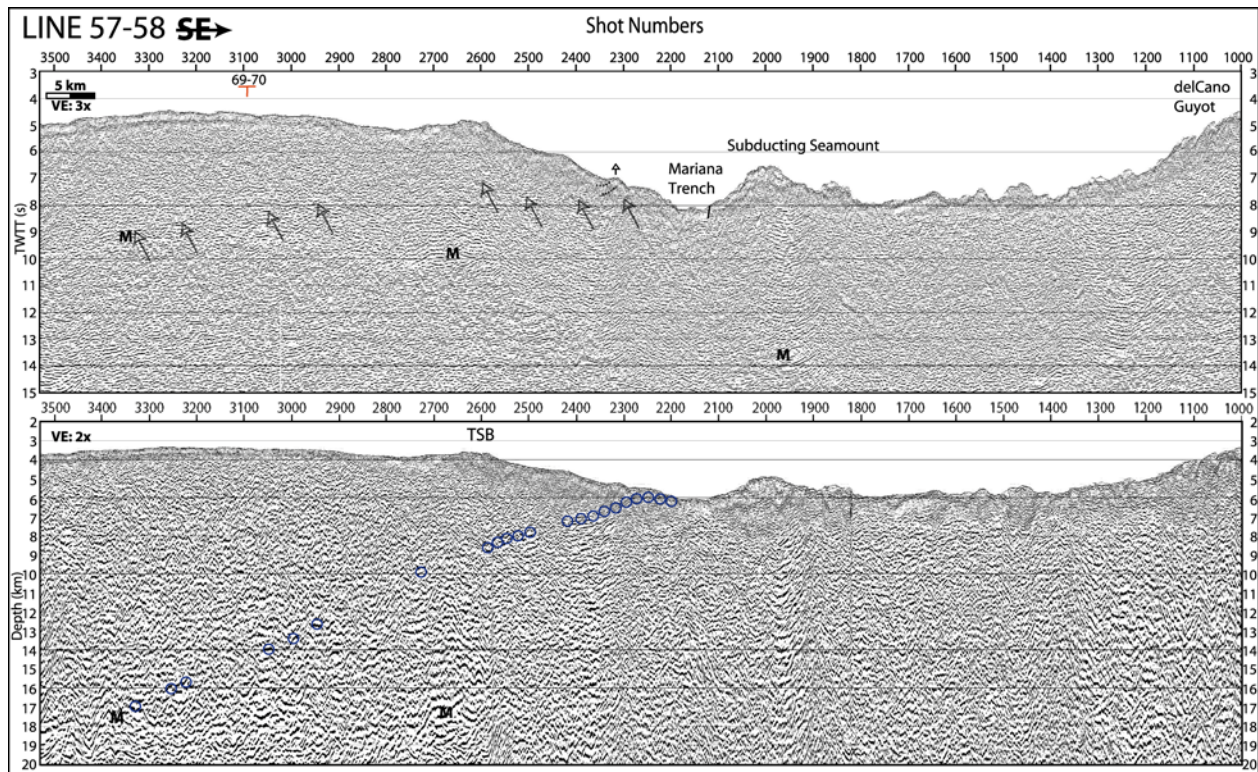
Figure 6. Time and depth sections of MCS Line 57–58. Symbols are the same as in Figure 2. This profile is representative of the Pacific Plate entering the Mariana Trench in Region C. The toe of the fore arc is uplifted as the flank of a Pacific Plate seamount subducts. TSB, trench slope break; M, seafloor multiple. Location on Figure 1.

bathymetric images are illuminated from the east to highlight relief.

4. Data Description

4.1. Incoming Pacific Plate and Mariana Trench

[19] The character of the subducting Pacific Plate and trench varies along the central Mariana margin (Figures 1 and 4) and can be divided into four regions on the basis of the morphology and structure seen on bathymetric and seismic profiles of the incoming plate (Figure 3). These four regions (A–D) are well-represented by MCS Lines 22–23, 53–54, 57–58 and 79–80 which, in this paper, we show from the incoming Pacific Plate to the outer Mariana fore arc (Figures 2 and 5–7).

[20] A bathymetry profile along the axis of the Mariana Trench reveals regional variations on the incoming plate (Figure 4). In both regions A and C, the trench floor shallows to <6 km because there are seamounts/ridges in the trench. Region B is characterized by the subduction of low-relief seafloor with a nearly constant trench axis depth of

8.5 ± 0.2 km. In Region D, the depth of the Mariana Trench increases toward the south from <8 km to >9 km. The outer trench slope of the incoming plate follows this same southward deepening trend.

[21] In Region A, (MCS Lines 22–23 and 47) the incoming plate is relatively smooth with a few seamounts and no large horsts or graben (Figures 4 and 5). Although the outer flexural bulge is ~200 km east of the trench axis, bending-related faulting begins ~95 km east of the trench near the 6 km depth contour (Figure 4). The faults in this region strike sub-parallel to the trench axis. Fault offsets are generally less than 200 m except for those bounding the trench axis graben. Seamounts enter the Mariana Trench in Region A near 18° and 18°30′N, locally steepening the outer trench slope.

[22] In Region B (MCS Lines 16–19 through 53–54), there are both trench parallel bending faults and faults striking NNE, oblique to the trench. The trend of the oblique faults is similar to that of the Mesozoic magnetic lineations identified by *Nakanishi et al.* [1992a] (Figure 1), therefore these fractures likely represent reactivated abyssal hill seafloor fabric. Profile 6 (Figure 4)
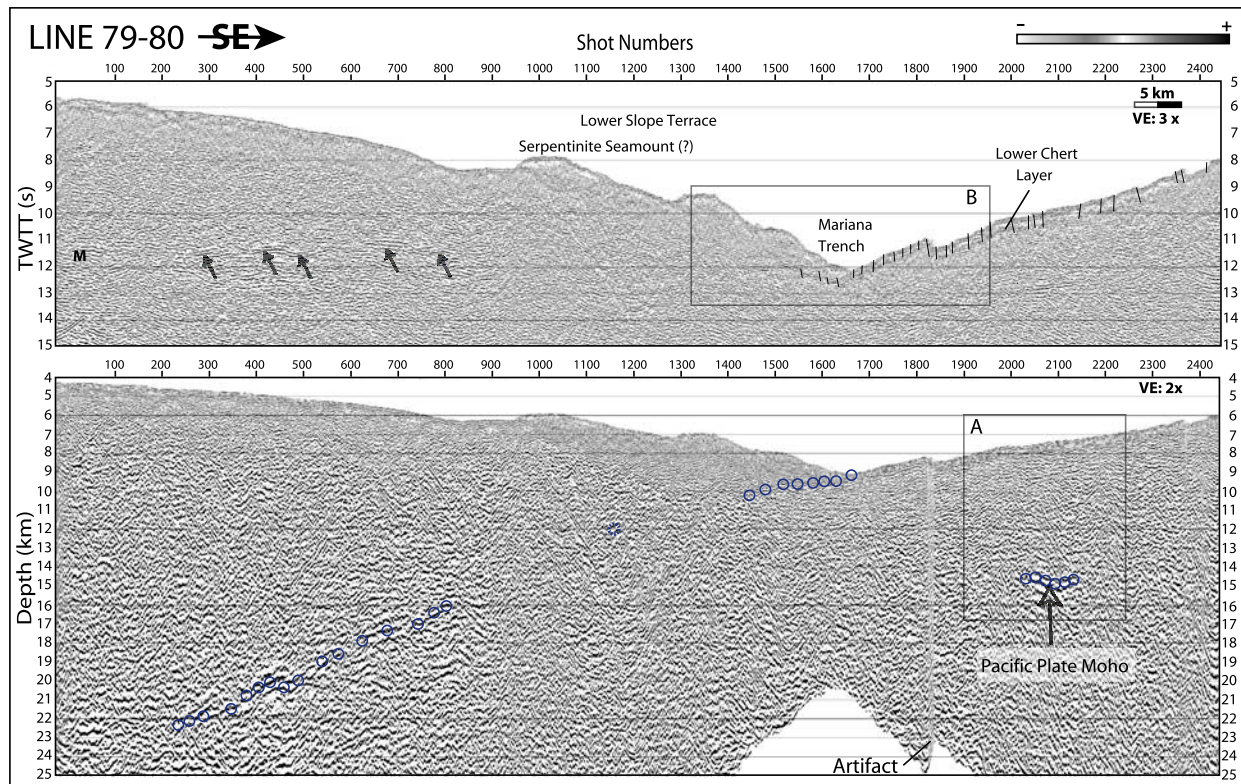
Figure 7. Time and depth sections of MCS Line 79–80. Symbols are the same as in Figure 2. The subducting plate reflection is obscured on the lower slope terrace beneath a possible serpentinite seamount. This profile is representative of Region D. Boxes A and B refer to the areas enlarged in Figures 10 and 11b. M, seafloor multiple. Location on Figure 1.

and Line 53–54 (Figure 2) cross graben formed by obliquely striking faults with a larger offset (~200 m) than those to the north. Much larger offset (400–700 m), trench-parallel faults occur proximal to the trench axis. In Region B flexural faults again begin near the 6 km contour, which varies southward from ~95 km east of the trench axis in the north to ~55 km on Line 53–54 (Figures 2 and 4).

[23] MCS Line 57–58 (Figure 6) lies within Region C which is characterized by the subduction of a fractured WNW-trending ridge and seamount chain (Figures 1 and 3). East of the delCano Guyot, the seafloor is flat with no visible offsets (Figures 3 and 4). West of the guyot, the seafloor is fractured and hummocky and, where visible, sediment and chert horizons are discontinuous (Figure 6). The trench shallows to nearly 5 km in this region and cusps to the west between Line 57–58 and Profile 5, but drops steeply to ~8 km on either side of the ridge (Figure 4).

[24] In Region D, the Pacific Plate bends steeply into the trench and the incoming seamounts are deformed by normal faults in response to plate

flexure (Figure 4). The trench curves to the SSW and the axis is roughly parallel to the oblique normal faults visible to the north. Fault offsets along Line 79–80 range from ~150–325 m (Figure 7). The trench floor, at >9 km, is the deepest in the study area (Figure 4).

4.2. Incoming Pacific Plate and Izu-Bonin Trench

[25] Bathymetric profiles across the Izu-Bonin Trench highlight differences between the subducting Pacific Plate in central Mariana and further north along the IBM margin (Figure 8). The incoming plate has few seamounts and is characterized by much larger offset normal faults (~500 m) and a more pronounced horst and graben morphology. As in the Mariana region, bending related faults begin ~100 km from the trench, near the 6 km depth contour; in contrast, however, nearly all of the flexural faults along the Izu-Bonin Trench are sub-parallel to the axis. The exception is the NNW trending graben imaged in the bathymetry and crossed by MCS Line Bonin 39 (Figure 9).
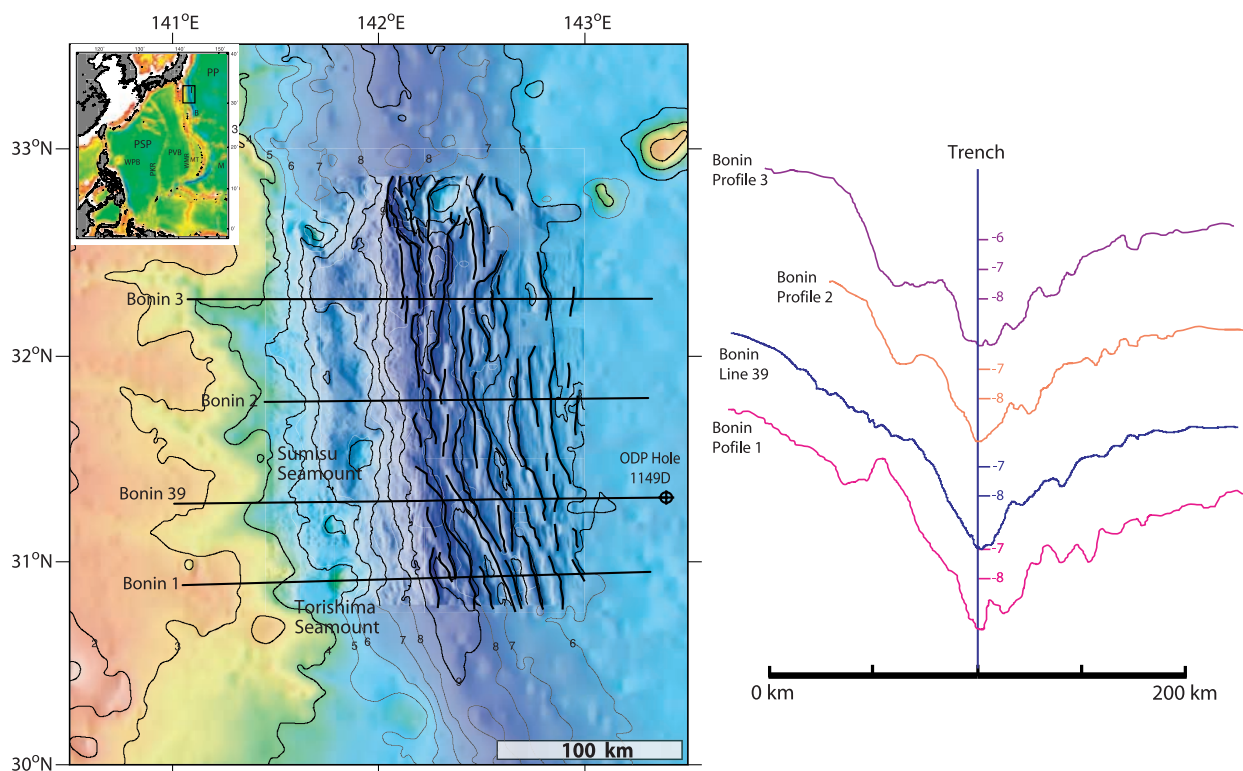
Figure 8. Izu-Bonin Trench bathymetry. Bathymetric profiles along MCS track Line 39 and computer-generated profiles across the Izu-Bonin Trench plotted from west to east. Flexure-related faults are outlined in black. VE~14x.

Bonin Line 39 reveals a trench floor that is deeper and wider than in central Mariana (Figure 9).

4.3. Pacific Plate Stratigraphy and Crustal Thickness

[26] Sediment and Pacific Plate crustal thicknesses vary along strike of the IBM margin (Figure 10) [*Abrams et al.*, 1993]. In the seismic sections, a lower-amplitude, discontinuous basement reflection is sometimes visible beneath the strong lower chert horizon, enabling us to calculate sediment thickness (Figure 10). Pacific Plate Moho occurs on three of the six trench-perpendicular Mariana MCS lines and along MCS Line Bonin 39 (Figure 10). East of the Izu-Bonin Trench, an ~0.3 km thick sediment package overlays basement and a Moho reflection is imaged ~6 km below the basement horizon. This seismic line crosses ODP Hole 1149D (Figures 8 and 10). East of the Mariana Trench, we image Moho in parts of Regions A, B and D. A strong chert layer reflection and discontinuous basement horizon are visible on Line 22–23 (Region A) where the sedimentary section is ~1 km thick. Moho is visible ~5.3 km below oceanic basement. To the south, along Line 53–54 (Region B), sediment and crustal thicknesses

increase. The doubling of the sediment package is likely because of volcaniclastic sediments shed from the surrounding seamounts (Figure 4) including the one shown to the west (Figure 10). On Line 79–80 (Region D), 0.5 km of sediments overlie a strong chert horizon and there is no basement reflection. Moho is located between 14 and 15 km depth.

4.4. Toe of the Inner Trench Slope

[27] Our seismic data across the toe of the inner trench slope allow us to determine to what extent accretion and/or sediment and seamount subduction occur along the central Mariana Trench. Lines 22–23 (Region A) and 57–58 (Region C) show deformation related to subducting seamounts. The incoming sediment and chert horizons are discontinuous and cannot be traced into the trench. There is evidence for uplift at the toe of the inner trench slope in a cross-sectional view and bowing up of the fore arc in the bathymetry as the leading edge of the seamounts subducts (Figures 1, 5, and 6). The subducting delCano Guyot is faulted and degraded west of 148°20′E (Figure 1).

[28] We interpret accretion at the toe of the inner trench slope along Line 16–19 (Region B)
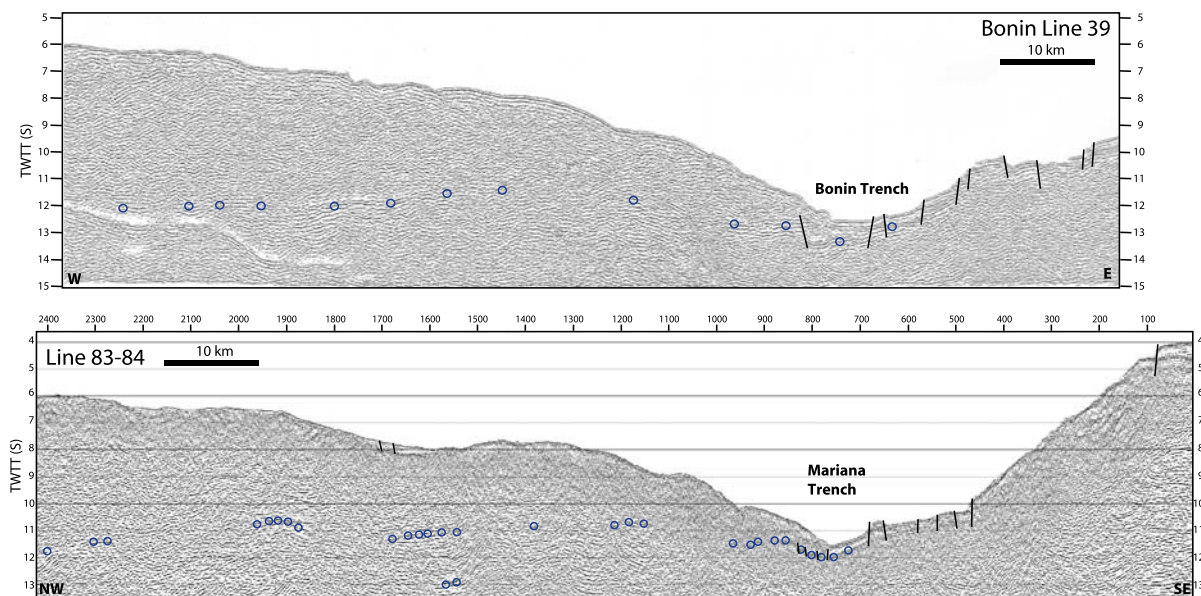
Figure 9. Time sections (3x) across the lower slope terrace of the Izu-Bonin and Mariana fore arcs. Hollow circles indicate the top of the subducting plate in time. Deeper circles on Line 83–84 represent picks along possible subducted plate mantle.

(Figure 11a). The incoming sediment package above the lower chert layer is thin, ~0.25 km and discontinuous reflections below this layer may represent basement. Line 16–19 has numerous low-angle, dipping reflections both at the distal toe of the slope and in the mound at the base of the inner trench slope. The top few 10s of meters of sediment are off-scraped at the toe of the slope by a frontal thrust terminating at the upper chert layer. A dipping reflection (shown in red), interpreted to be a thrust fault, terminates at the lower chert horizon near Shot Point (SP) 12287 and separates the two packages of dipping horizons. The lower chert layer is visible west of the trench axis beneath the dipping reflections to near SP 12100. The dipping reflections on Line 16–19 were not removed by migration tests and are also visible in stacked data, suggesting that these are real features and not noise introduced by migration. A package of slope sediments (yellow) covers the top of the deformed sediments at the toe, and we interpret other pockets of thin sediments to the west. Interspersed with the dipping reflections are discontinuous horizons with a near-horizontal or slightly east-dipping slope.

[29] We interpret complete sediment subduction beyond the toe of the inner trench slope along Line 53–54 (Region B) (Figure 11a). The wide trench floor is formed by the subduction of a large graben complex and is underlain by ~0.5 km of oceanic sediment. There is negligible trench fill. The top of the sediment package and both chert layers are visible beneath the toe of the inner trench slope up to 10 km west of the trench axis.

[30] In Region D, both Lines 83–84 and 79–80 are characterized by highly faulted incoming sediments ~0.5 km thick and a strong, faulted lower chert layer visible beneath the toe of the slope (Figure 11b). Beneath the toe of the slope there are normal fault offsets in the lower chert horizon and sediment layers. On Line 83–84 the incoming sediment package thickens beneath the toe of the slope and reflections are slightly folded. The lower chert layer shallows to the west through a series of stair-stepping normal faults, reaching a high less than 9 km deep. We image both horizontal and low-angle dipping reflections at the toe of the inner trench slope; however, we are unable to resolve coherent sediment packages west of the trench axis.

[31] On Line 79–80 (Figure 11b) graben separated by SE-dipping normal faults subduct beneath the inner trench slope. Reflections parallel to the faulted chert layer and horizontal reflections are visible beneath the toe of the slope. There is no evidence for thickening of the sediment package.
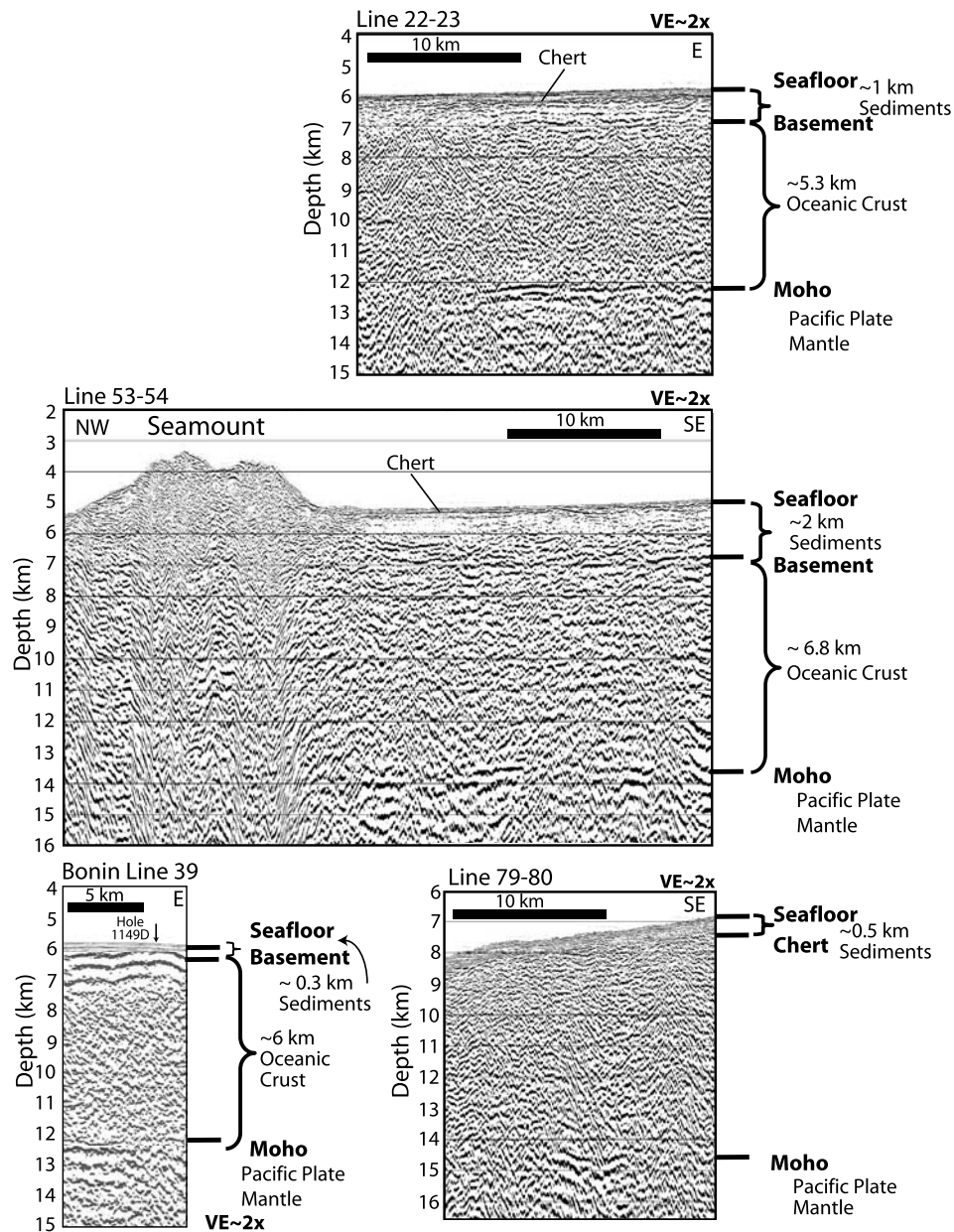
Figure 10. Portions of seismic lines showing Pacific Plate inputs. Locations of Mariana blowups are shown on Figures 1, 2, and 7.

Sediments and both chert layers subduct past the trench; however, only the lower chert horizon can be resolved beyond 5–7 km west of the axis.

4.5. Inner Trench Slope

[32] The bathymetric map and profiles on Figure 4 illustrate along-strike variations on the inner trench slope of the central Mariana system. In Region A the inner trench slope is steep (~8.5°), with no visible faults or significant sediment east of the

trench slope break (SP 2900) (Figure 5). Further west on Line 22–23, high-angle normal faults offset seafloor and sediments less than 0.5 km thick in a 38-km wide basin between two basement highs. In Region B, Line 16–19, which images fore arc in between structural highs, is characterized by nearly flat seafloor at ~4 km depth until ~35 km west of the trench where it bends and plunges into the trench with a slope of ~6.5° (Figure 4). Further south in Region B, profiles 2 and 53–54 show a more gradual descent along the
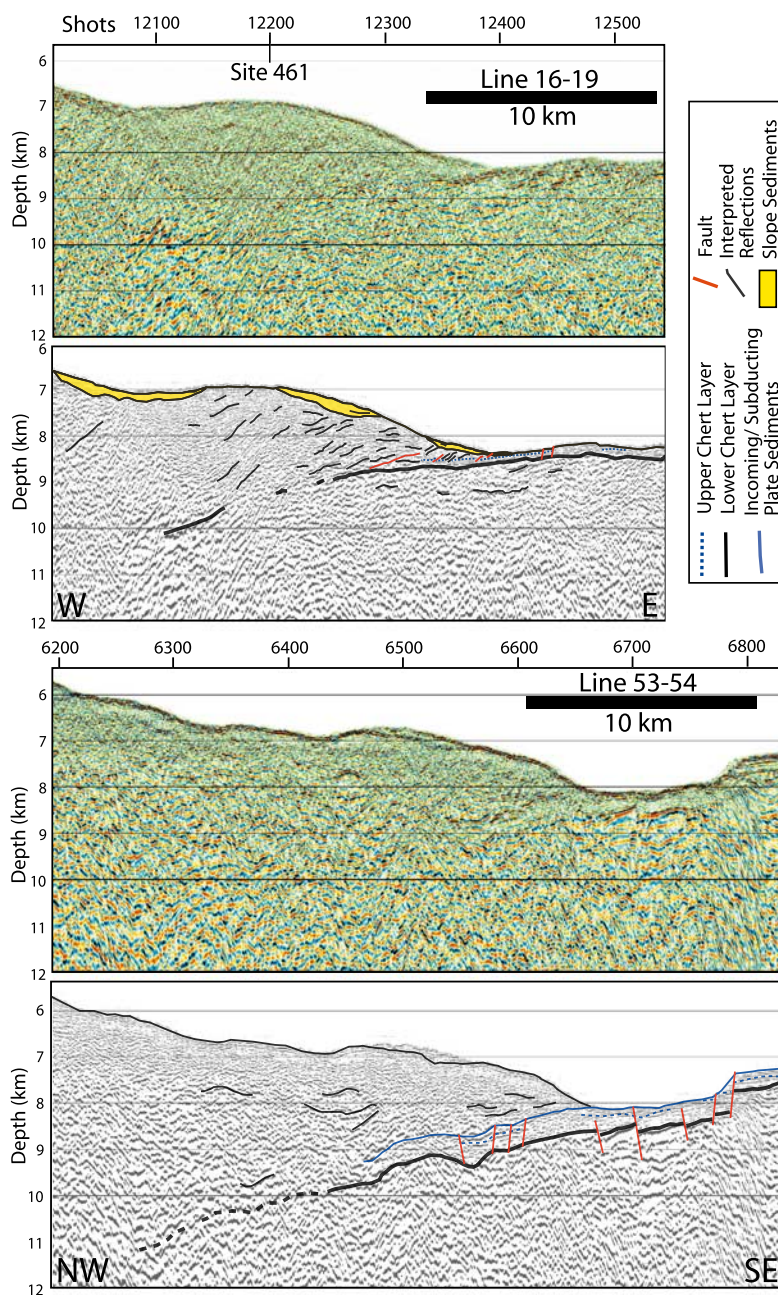
Figure 11a. Depth and interpreted depth sections (2x) across the toe of the lower trench slope along Lines 16–19 and 53–54 in Region B of the Mariana Trench. The upper and lower chert horizons are visible on each line. Line 16–19 shows thickening and accretion at the toe of the slope. There is complete sediment subduction along Line 53–54.

inner trench slope (~5.3°). On Line 53–54 a 0.8 km thick sediment package is visible beneath and to the west of the flank of Celestial Serpentinite Seamount (Figure 2). These sediments are overthrust by a mound buttressing Celestial Seamount to the east that is likely to be another serpentinite seamount [*Oakley et al.*, 2007]. Basement exposure begins near SP 5850 and continues down the inner trench slope (Figure 2). On Line 57–58 (Region C),

which crosses Celestial Ridge (the bathymetric high upon which Celestial Seamount is built), we see a thin (<400 m) section of fore-arc sediments that pinches out near SP 2900, exposing basement on the trench slope break (SP 2600) and down the narrow (20 km) inner trench slope (Figure 6).

[33] Fore-arc morphology and profiles across it are distinctly different south of ~15°N in Region D. A good example is Line 79–80 (Figure 7) which has
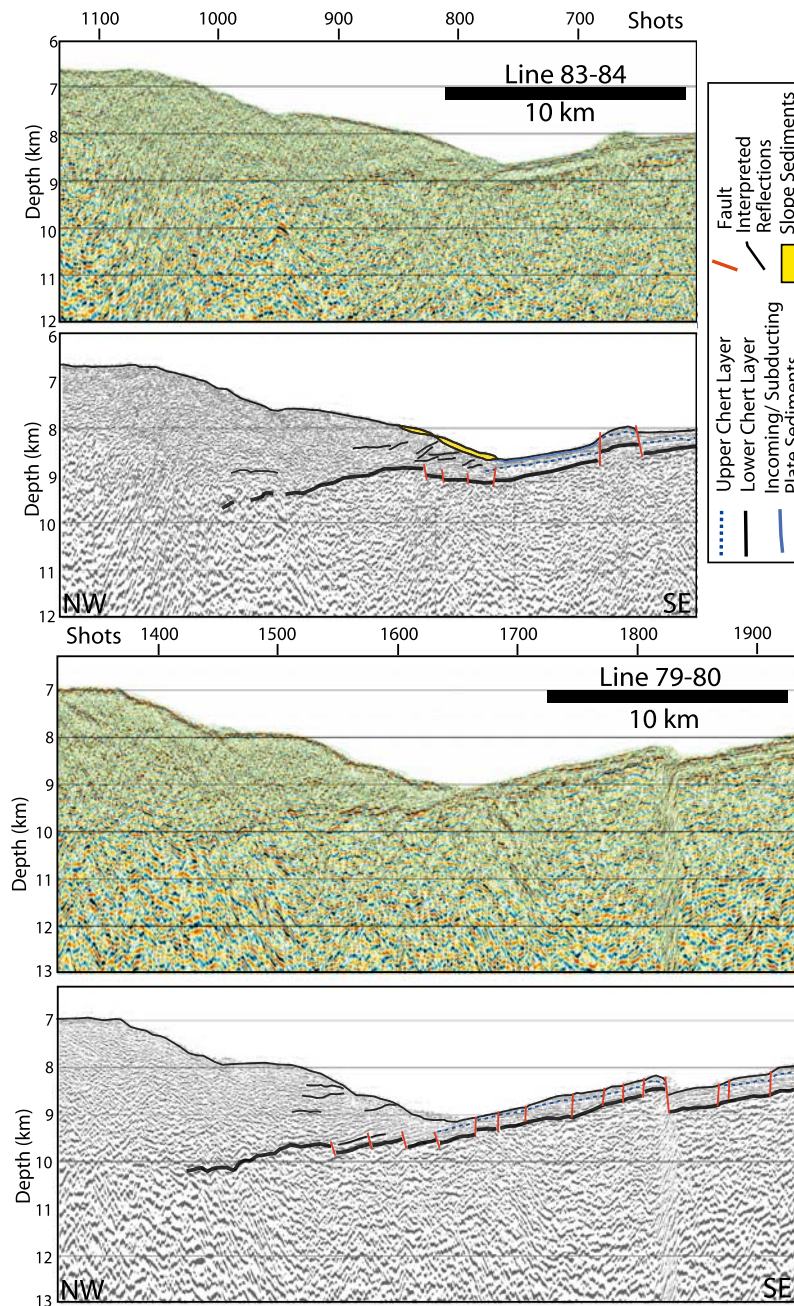
Figure 11b. Lines 83–84 and 79–80. Incoming Pacific Plate sediments and both chert layers are offset by normal faults.

no trench slope break but instead slopes gradually from the fore-arc basin to a lower slope terrace (outlined by a dashed line on Figure 4). This region lacks the large fore-arc highs present in the north. There is a thin, <0.3 km, veneer of sediments draping the outer fore arc.

[34] Seismic and bathymetric profiles along the inner trench slope in Region D closely resemble profiles across the Izu-Bonin fore arc (Figures 8

and 9). The Izu-Bonin region has a well-defined lower slope terrace with serpentinite seamounts. Line 79–80's profile is similar to that of Bonin Profile 1 which crosses Torishima Serpentinite Seamount. The section along Line 83–84 closely resembles Bonin Profile 2, whereas Bonin Line 39 crosses the lower slope terrace between two serpentinite seamounts (Figure 9). The lower slope terrace along both margins has little sediment cover. Aside from the small high-angle normal
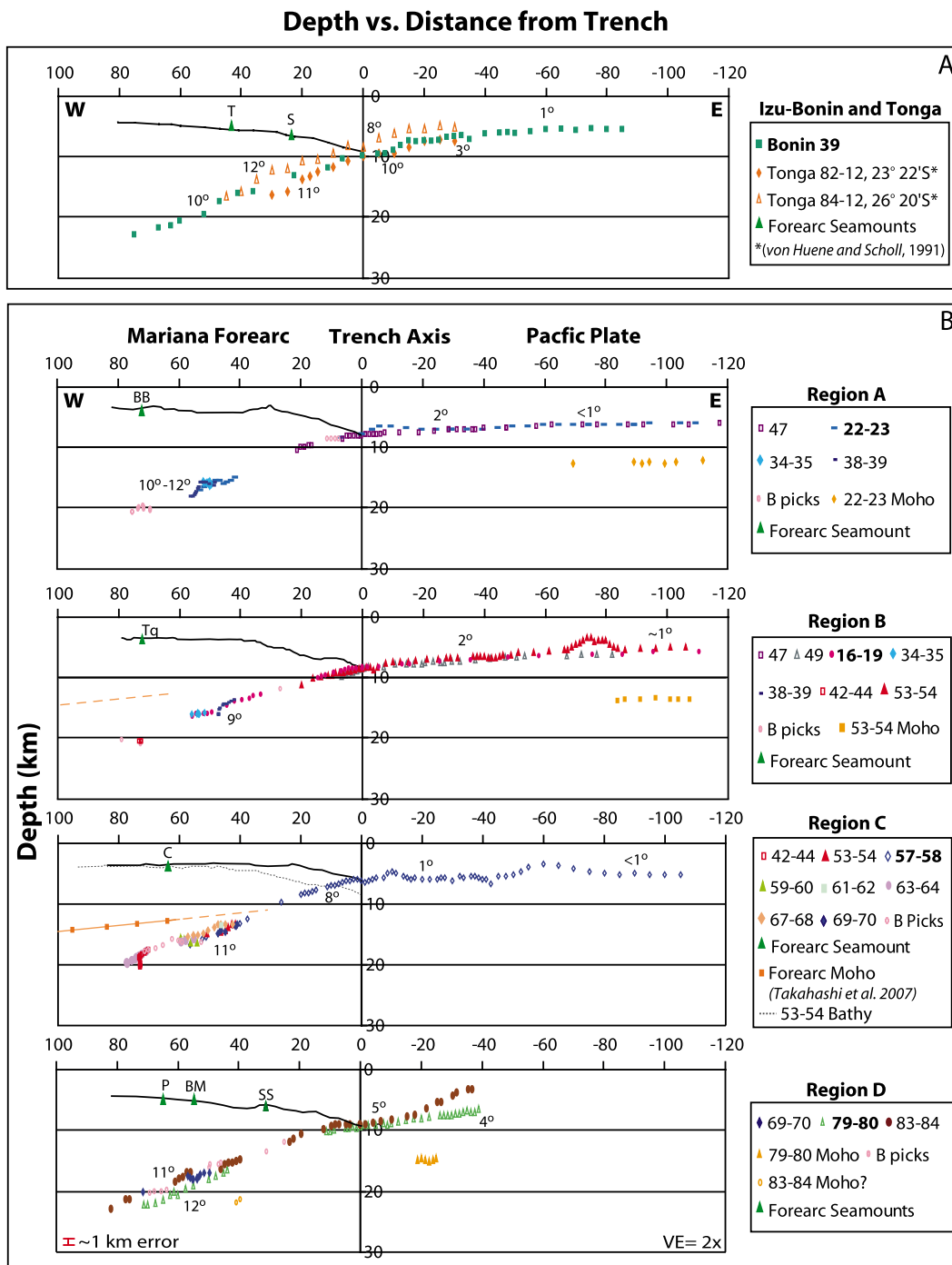
Figure 12. The incoming Pacific Plate chert layer and top of subducted plate plotted in depth versus distance from the trench by MCS profile number. (a) Izu-Bonin and Tonga Trenches. (b) Central Mariana Trench by region (defined on Figure 3). Pacific Plate Moho is visible on Lines 79−80, 83−84, 53−54, and 22−23. Green triangles represent the base of the serpentinite seamounts: BB, Big Blue; Tq, Turquoise; C, Celestial; P, Peacock; BM, Blue Moon; SS, Possible Serpentinite Seamount; T, Torishima Seamount; S, Sumisu Seamount. Black lines are representative bathymetric profiles across the fore arc in each region (source profile is shown in bold). Subducting plate dips are labeled. Fore-arc bathymetry along Line 53−54 and Moho from the refraction line of *Takahashi et al.* [2007] are shown in Region C. Moho is extrapolated to Region B (dashed orange line).
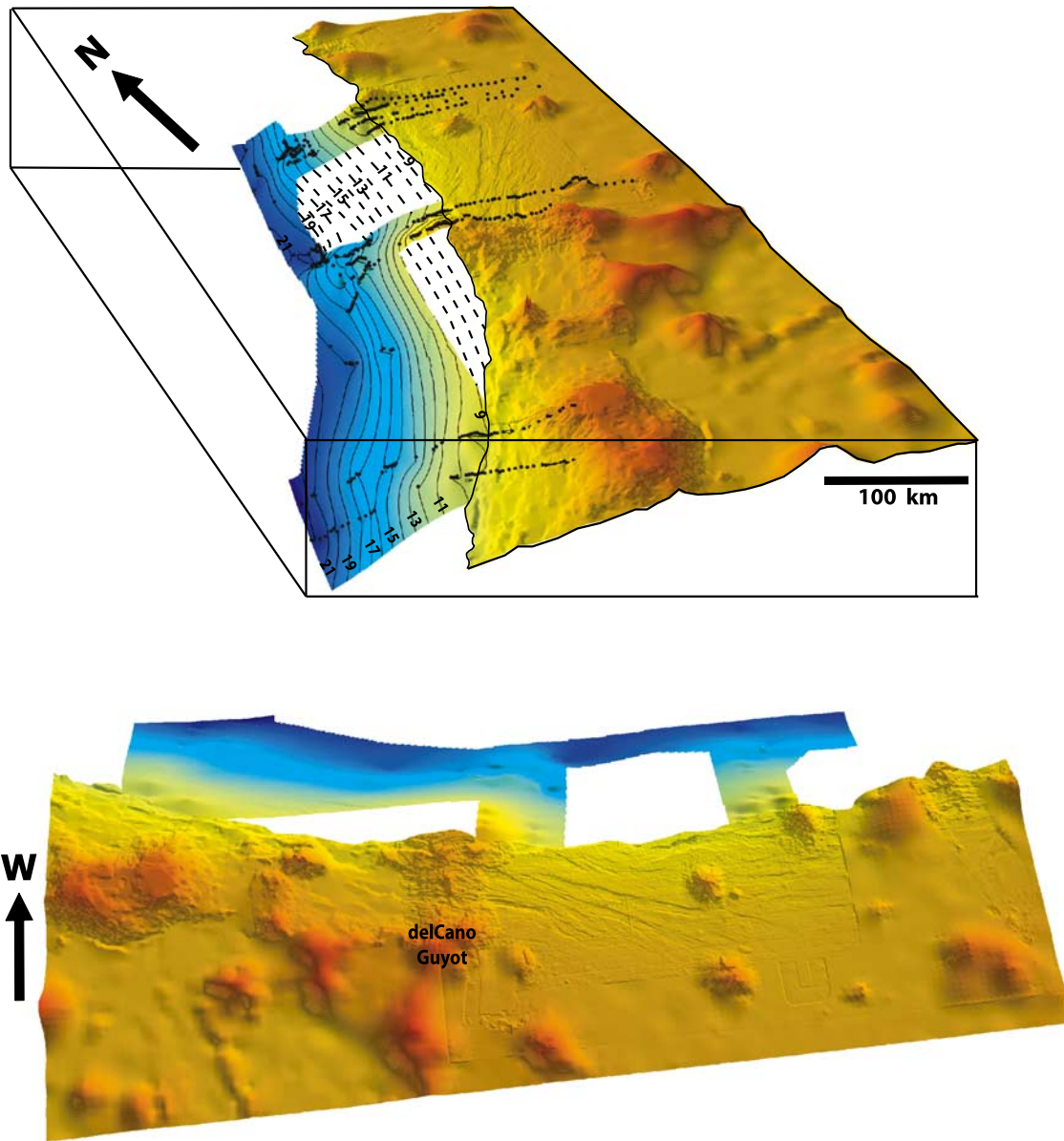
Figure 13. Three-dimensional images of the subducting Pacific Plate. Black dots represent top of plate-depth picks and Pacific Plate chert layer picks. Contours and subducting plate surface were created in ArcGIS. Contour interval is 1 km. VE = 3x.

faults offsetting sediments in a slope basin on Line 83–84, there are no visible faults that would account for the subsidence or marked deepening in these regions of the outer IBM fore arc.

4.6. Outer Mariana Fore Arc and Depths to the Subducting Plate

[35] Several serpentinite seamounts located between $14°–18.5°N$ lie in a narrow swath of fore arc 30–70 km from the trench axis (Figure 1). We created a bathymetric profile parallel to the trench axis and east of the line of serpentinite seamounts

(shown in crimson on Figure 4) to illustrate potential influences on the morphology of the fore arc from the subducting plate. The southward deepening trend along the trench axis in Region D is roughly mirrored by the overriding fore arc. In Regions A and C, shallow trench morphology corresponds with highs on the outer fore arc; however, not all of the bathymetric highs visible on the fore-arc profile appear to correlate with highs on the incoming plate such as the large (>2 km tall) feature at $17°20'N$ in Region B. The origin of this structure is unknown and it was not transected by our survey.

[36] Beneath the outer Mariana fore arc there is a prominent, low-frequency reflection from the top of the subducting plate, visible on 17 seismic profiles (Figure 1). A similar reflection is also imaged on Bonin Line 39 (Figure 9). On the MCS lines shown, hollow circles represent depths to the top of the plate. In addition to the subducted plate, on Line 83–84, at ~13 s TWTT, there is a prominent, discontinuous reflection that may represent subducted Pacific Plate Moho (Figure 9). On several seismic lines the top of the subducting plate is visible below the flanks of serpentinite seamounts on the outer fore arc, although it is not imaged directly beneath the edifices (Figure 3).

[37] We use our interpretations of depths to the top of the subducted plate across the entire central Mariana fore arc and depths to the lower chert layer on the Pacific Plate east of the trench to map subducting plate morphology on both sides of the trench (Figures 12 and 13). We plot depths across the Izu-Bonin Trench along with existing data from the Tonga Trench for comparison (Figure 12a). The subducted plate along the Izu-Bonin margin and the northern Tonga margin dips 10–11° beneath the fore arc. The top of oceanic crust on Tonga Line 84–12 is shallower and steeper (12°) beneath the fore arc than the other two lines. Unlike central Mariana, both Izu-Bonin and Tonga are characterized by the subduction of large offset horsts and graben.

[38] Along-strike the central Mariana margin there are variations in the profile of the subducting Pacific Plate (Figure 12b). In Region A, the relatively smooth incoming plate bends gently into the trench axis and a seamount locally increases the dip of the outer trench slope. The plate reaches ~20 km depth beneath Big Blue Serpentinite Seamount. Seismic Line 53–54 crosses from Region B into Region C (Figure 3). The morphology of the incoming plate is typical of Region B; however, plate depths beneath the outer fore arc plot within Region C. Overall the plate is shallower in Region C likely because of the subducting delCano ridge (Figures 3 and 6). Deformation caused by a subducting bathymetric high is consistent with the shallower trench floor (Figure 4) and the westward deflection of the trench axis seen in Region C (Figure 3). In Region D, the outer trench slope on Lines 83–84 and 79–80 is steepened as the western flank of the Victoria Guyot approaches the trench axis (Figure 3). The subducted plate on Line 79–80 is slightly steeper and 1–2 km deeper than on Line 83–84 (Figure 12b).

The seafloor is deepest in this region of the outer Mariana fore arc, providing the best and most extensive images of the subducted plate un-obscured by the seafloor multiple (Figures 7 and 9). On Line 79–80, the subducted plate penetrates 22 km depth within a distance of 70 km from the trench, illustrating that the plate, along with the trench, is also deepest in Region D. Across the central Mariana margin, the subducting plate dips 9–12° beneath the serpentinite mud volcanoes. Depth to the plate beneath the base of the serpentinite seamounts decreases from ~17 km (Big Blue) to 7 km (SS) with shallowest depths closest to the trench (Figure 12b).

[39] The regional variations in morphology of the Pacific Plate subducting beneath the central Mariana fore arc are well illustrated in three dimensions (Figure 13). The subducted plate is not a simple curvi-planar surface. Although the dip of the plate beneath the outer fore arc is relatively constant across the 4 regions (9–12°) (Figure 12b), there are isolated highs and regional undulations. The plate is shallowest in Region C, west of the delCano Guyot, and deepest in Region D beneath the lower slope terrace.

5. Discussion

5.1. Flexure of the Incoming Pacific Plate and Its Failure at the Mariana Trench Graben

[40] The Pacific Plate with its superposed seamounts is offset by plate flexure normal faults (Figures 4, 8, and 13). Normal faults begin near the 6 km depth contour at ~55 km and ~95 km east of the trench on Lines 53–54 and 22–23, respectively (Figures 2 and 4). Where the Pacific Plate fabric strikes more than 25° from trench-parallel (e.g., north of ~17°40′N), new faults are formed during bending, whereas abyssal hill faults are preferentially reactivated when this angle is less than 25° (Figures 1 and 4), as is seen globally [Billen et al., 2007]. In Region B we observe both reactivated abyssal hill fabric and new trench parallel faults as a function of the changing azimuths of the trench axis and plate fabric (Figures 1, 3, 4, and 13).

[41] Bending related faults begin ~100 km east of the trench on Bonin Line 39, again near the 6 km contour (Figure 8). In contrast to the Mariana system, nearly all of the flexural faults along the Izu-Bonin Trench are sub-parallel to the axis,

consistent with the observation that magnetic anomaly lineations strike sub-perpendicular to the trench [*Nakanishi et al.*, 1992a] and therefore abyssal hill fabrics are not reactivated. A large relief NNW trending graben south of 31°25′N is an exception to this and is likely a reactivated fracture zone (Figure 8).

[42] Flexural fault offsets along the Izu-Bonin margin are commonly ~500 m, similar to large-offset horsts and graben in other margins like Middle America and Tonga [*Bodine and Watts*, 1979; *Lonsdale*, 1986; *Ranero et al.*, 2003], whereas, in the Mariana system, outside of the trench graben, maximum offsets are rarely 300 m (compare Figures 4 and 8).

[43] Large normal fault offsets (500–700 m) of the subducting plate in the Mariana system occur typically within ±10 km (maximum 15 km) of the trench axis (Figures 1, 4, and 11). The Mariana Trench axis is commonly a graben (Figures 2, 4, and 11). There is an abrupt change in Pacific Plate dip from <4° (mostly ≤2°) at ~10 km east of the trench axis to >8° by 10 km to the west (Figure 12b). This significant change of dip in such a short distance relative to the plate flexural wavelength suggests that the plate fails rather than simply bends under the applied loads. We infer that the trench graben is the surficial structural expression of plate rupture which has been proposed to occur in response to the pull of the downgoing slab [e.g., *Kanamori*, 1971, 1986; *Abe*, 1972; *Ammon et al.*, 2008]. We are unable to image the normal faults to depth and we do not have any direct evidence of the corresponding mid-lower plate failure mechanism.

[44] The Izu-Bonin Trench axis is also a graben (Figures 8 and 9); however, the abrupt change in plate dip occurs ~20 km east of the trench axis (Figure 12a). This is also true along the Tonga Trench. Large offset horsts and graben occur along the outer trench slope in Tonga and Izu-Bonin but are not restricted to within 10 km of the trench axis as we observe in Mariana (Figure 12). For all three intraoceanic margins the change in the dip of the incoming plate corresponds to the formation of large offset graben. We propose that for these margins the sharp change in plate dip corresponds to the creation of large offset normal faults where the plate fails rather than flexes [e.g., *Kanamori*, 1971; *Abe*, 1972].

[45] Seismic reflection data from New Zealand along the Hikurangi Subduction Zone show a kink in the subducting Pacific Plate at ~120 km from the trench axis [*Henrys et al.*, 2006]. The change in dip of the plate (from 3° to >15°) coincides with the onset of intraplate seismicity. Earthquakes near the plate interface have low-angle thrusting mechanisms, whereas focal mechanisms show normal faulting events within the crust of the subducting plate. *Henrys et al.* [2006] propose that the sharp change in dip of the subducting plate is caused by simple shear on reactivated steeply dipping normal faults "akin to the down-stepping motion of an escalator."

[46] Pacific Plate subduction along the Japan Trench is also characterized by a sharp change in plate dip [*Ito et al.*, 2004, 2005; *Fujie et al.*, 2006]. This increase in dip (from 5°–13°) occurs approximately 70–80 km landward of the trench axis [*Fujie et al.*, 2006] and corresponds with the updip limit of rupture zones of large earthquakes [*Ito et al.*, 2005].

[47] The kinks in plate dip (Hikurangi, Tonga, IBM, and Japan), and the few great (>M8) normal faulting earthquakes at subduction zones (Sanriku, 1933; Sumba, 1977; Kuril, 2007) occur seaward of the updip limit of rupture zones of large earthquakes or in regions of weak seismic coupling, where and/or when slab pull forces can operate unimpeded by interplate frictional coupling on the subducting plate [cf. *Ammon et al.*, 2008].

5.2. Inputs to the Mariana Subduction Factory

[48] In order to correctly quantify the inputs delivered to the Mariana subduction factory, we need to understand the processes (subduction, accretion, erosion, and underplating) that affect the toe of the system. Our interpretation of Lines 53–54 and 79–80 suggests complete subduction of the entire ~0.5 km thick sedimentary section (Figures 11a and 11b). There is no current offscraping at the toe of the slope. The trench floor is deep (>8 km) and wide and contains little to no ponded sediment.

[49] The toe of the slope on Lines 16–19 and 83–84 show evidence for sediment accretion in Regions B and D (Figures 11a and 11b). On Line 83–84 sediments within a graben beneath the distal toe of the slope are folded and thickened, indicating horizontal compression. The presence of low-angle, arcward-dipping reflections suggests that some material above the lower chert layer may be incorporated into thrusts and accreted. On Line 16–19, the top 10–20 m of sediment is off-scraped at the distal

edge forming a small accretionary wedge. The upper chert layer subducts beneath the outer toe, but may become underplated further toward the arc where a larger fault offsets sediments down to the lower chert horizon (Figure 11a). Arcward-dipping reflections between SP 12100 and 12250 suggest that thrusting occurs west of the toe of the slope.

[50] DSDP Site 461 was drilled 20.5 m into a small ridge at the base of the inner trench slope on Line 16–19 (Figures 1 and 11a). DSDP Leg 60 scientists inferred, on the basis of the island arc affinities of the materials recovered, that the ridge is part of a large slump extending into the trench [*Hussong and Uyeda*, 1981b]. The discovery of calcareous sediments at Site 460 (also along the inner trench slope below the modern CCD) (Figure 1), led them to propose that significant subsidence has occurred on the outer Mariana fore arc, implying erosion of the margin [*Hussong and Uyeda*, 1981b]. We conclude, however, on the basis of the current evidence for accretion at the toe and the low-angle dipping reflections within the ridge on Line 16–19, that it is primarily an accretionary structure made up of thrust packages of accreted sediments. Thin slope sediments are present in isolated packages along the inner trench slope and on top of the accretionary wedge. It is likely that Leg 60 drilling only penetrated these sediments, which would be mostly material derived from exposures on the upper part of the inner trench slope and transported downslope. Near-horizontal to E-dipping reflections imaged within the wedge may be created by slope sediments or slump packages of slope sediments (Figure 11a). Our interpretation does not support subsidence and erosion in Region B.

[51] Although the interpretation of accretion of sediments less than 1 km thick along Line 16–19, and possibly along 83–84, appears inconsistent with the global trend seen by *von Huene and Scholl* [1991] and *Clift and Vannucchi* [2004], this may be a question of scale. Small-scale accretion at the toe of the inner trench slope does not classify the central Mariana margin as accretionary. Subduction in the Mariana system began 50 million years ago [*Taylor*, 1992; *Cosca et al.*, 1998]. If the entire sedimentary section above the lower chert layer (~0.25–0.5 km thick) was consistently accreted over this time we would expect to see a much larger accretionary prism along the Mariana Trench. For example we can calculate the potential size of an accretionary wedge along the central Mariana subduction zone using the method described by *von Huene and Scholl* [1991]. Assum-

ing an average subduction rate of 45 km/ma over the last 50 Ma, and complete accretion of a 0.25 km thick sediment package with an average initial porosity of 40%, the accretionary prism would cover 337.5 km^2/km of trench. The size of the small prism along Line 16–19 is less than 20 km^2, suggesting that this is not a long-lived or constantly accreting feature. The only evidence for accretion in the Mariana subduction zone is at the toe of the inner trench slope and these small accretionary prisms are likely to be ephemeral features. We found no evidence for thrusting further upslope.

[52] We interpret the horizon representing the lower chert layer to be subducting beneath the toe of the fore arc throughout the study area. This layer is not offset by thrust faults, therefore we assume that it, along with any sediment (volcaniclastics/claystones) between chert and igneous basement, are subducting along all four regions of the central Mariana Trench. Our data do not image sediments farther than ~10 west of the trench, therefore it is possible that sediments subducting beyond the toe of the slope may become underplated beneath the fore arc. However, the sediment section entering the Mariana Trench is thin and geochemical data from the active arc argue against underplating. Both subducted sedimentary and oceanic crustal components are identifiable in erupted Mariana arc basalts, and the basalts follow the global trend in Ba sediment input versus Ba arc output [*Elliott et al.*, 1997], suggesting that at least some Pacific Plate sediments reach the zone of magma generation.

[53] Our interpretations show that, with the exception of small-scale accretion at the toe of Line 16–19, the entire incoming sedimentary section is being subducted beyond the fore-arc region. These interpretations and comparison with the drilling results from IODP Hole 801C in the Western Pacific allow us to quantify the inputs to the Mariana subduction system (Figure 10). The thickness of the incoming sediment section on the Pacific Plate between 14° and 19° N ranges from 0.5 to 2 km. Oceanic crust in Region B is 6.8 km thick, compared with 5.3 km near 18°N in Region A and 6 km in the Izu-Bonin region. If the lower chert layer on Line 79–80 (Figure 10) is in contact with or representative of the top of oceanic crust, then crustal thicknesses in Region D are also ~7 km. The thickened crust may be related to the numerous, large seamounts in these regions (Figure 1). Igneous intrusions can locally thicken the crust and/or large seamounts may depress Moho.

[54] Along Line 53–54, in Region B, the complete sediment section (likely similar to that described above for Hole 801C), along with ~7 km of oceanic crust are being subducted. The average water content and porosity, calculated from measurements of wet and dry weights and dry volume, of the sedimentary section drilled at Site 801 are 22% and 40%, respectively [*Shipboard Scientific Party*, 1990]. On the basis of these numbers and assuming complete compaction by 15 km depth, 1 m^2 of 500 m thick subducted Pacific Plate sediment will lose 107–195 g of water. *Schmidt and Poli* [1998] suggest that a vertical, 1 m^2 section of 7 km-thick oceanic crust releases $8 \pm 2 \times 10^6$ g H2O/km depth from 20 to 70 km. In addition, fault planes formed by plate flexure may create pathways for fluid to enter the subducting oceanic crust; however, this amount is difficult to quantify [*Ranero and Sallares*, 2004]. The top of the subducted Pacific Plate is ~20–22 km deep near the majority of the larger serpentinite seamounts (e.g., Big Blue, Turquoise and Peacock). The amount of water released by pore space compaction of incoming sediments is insignificant compared to the amount of water contained in the subducting altered igneous oceanic crust. However, if the oceanic crustal section does not begin to dewater until depths greater than 20 km [*Schmidt and Poli*, 1998], then the incoming sediment section controls fluid release beneath the outer fore arc (Figure 12b). Therefore, complete accretion of the sedimentary section above the lower chert layer, as seen along Line 16–19, will result in a local decrease in the amount of water released beneath the serpentinite seamounts.

[55] Although the subducted Pacific Plate is nearly vertical beneath the Mariana arc, its dip is shallow more than 80 km west of the trench, which has a large effect on estimates of the amount of water released beneath the outer fore arc and the amount of mantle wedge that is hydrated. In their recent publication, *Savov et al.* [2007] use a subduction angle of 20°, extrapolated from earthquake seismicity [*Stern et al.*, 2003], to calculate the volume of mantle beneath the Mariana fore arc. Our results show that the dip of the subducting plate does not exceed 12° more than 80 km west of the Mariana and Izu-Bonin Trenches (Figure 12). The velocity models used to depth convert our MCS data were based on seismic refraction studies across the Mariana and Izu-Bonin fore arcs [*LaTraille and Hussong*, 1980; *Kamimura et al.*, 2002; *Takahashi et al.*, 2007]. The Takahashi model is coincident with Line 53–54 which allowed us to relate layer thicknesses and velocity gradients in the model

directly to the seismic data (Figure 2). Our estimates of subducting plate geometry determined from these depth sections are more accurate than previously published values based solely on earthquake data. *Savov et al.*'s [2007] use of a plate dip 8° greater than our calculations results in a significant overestimate of the thickness of the mantle wedge between the plate and the fore-arc crust and the amount of water released beneath the serpentinite seamounts.

5.3. Subducting Pacific Plate Seamounts and the Inner Trench Slope

[56] New data from the Mariana subduction zone provide an excellent example of active seamount subduction (Figures 5, 6, and 13). The seamounts near Lines 22–23 (Region A) and 57–58 (Region C) are in a similar stage of subduction to the Daiichi-Kashima Seamount in the Japan Trench [*Lallemand et al.*, 1989]. The toe of the inner trench slope is uplifted as the flank of a seamount begins to subduct [see *Yamazaki and Okamura*, 1989, Figure 10b]. Fore-arc material is translated arcward and upward, resulting in the westward migration of the trench axis in map view (Figure 13). When the seamount has subducted completely, the oversteepened inner trench slope will slump and deform until it reaches a stable condition [*Lallemand and Le Pichon*, 1987; *von Huene and Culotta*, 1989]. Slumped sediments from the upper slope that reach the trench may be reaccreted to the margin, or subducted, effectively removing material from the overriding plate. The trench floor is shallowest in Region C, possibly because of slumped material from the oversteepened inner trench slope, as well as the presence of deformed incoming seamounts.

[57] The inner trench slope along the central Mariana system is primarily composed of fore-arc basement with little sediment cover except in isolated pockets. We did not image any large faults. According to *Bloomer and Hawkins* [1983], serpentinized ultramafic rocks are an important component of the inner slope as they occurred in 10 of 19 dredges ranging from the bottom of the trench up to the trench-slope break. Dredges reveal ~40% serpentinized ultramafic rocks from the inner slope in Regions A and B between Lines 22–23 (SP 2400–2500) and 16–19 (SP 12100–12200) and in Region D near 16°45′N [*Bloomer and Hawkins*, 1983] (Figure 1). These may be derived from serpentinite mud volcanoes upslope in these areas (e.g., Big Blue, Peacock, Blue Moon). Alternative-
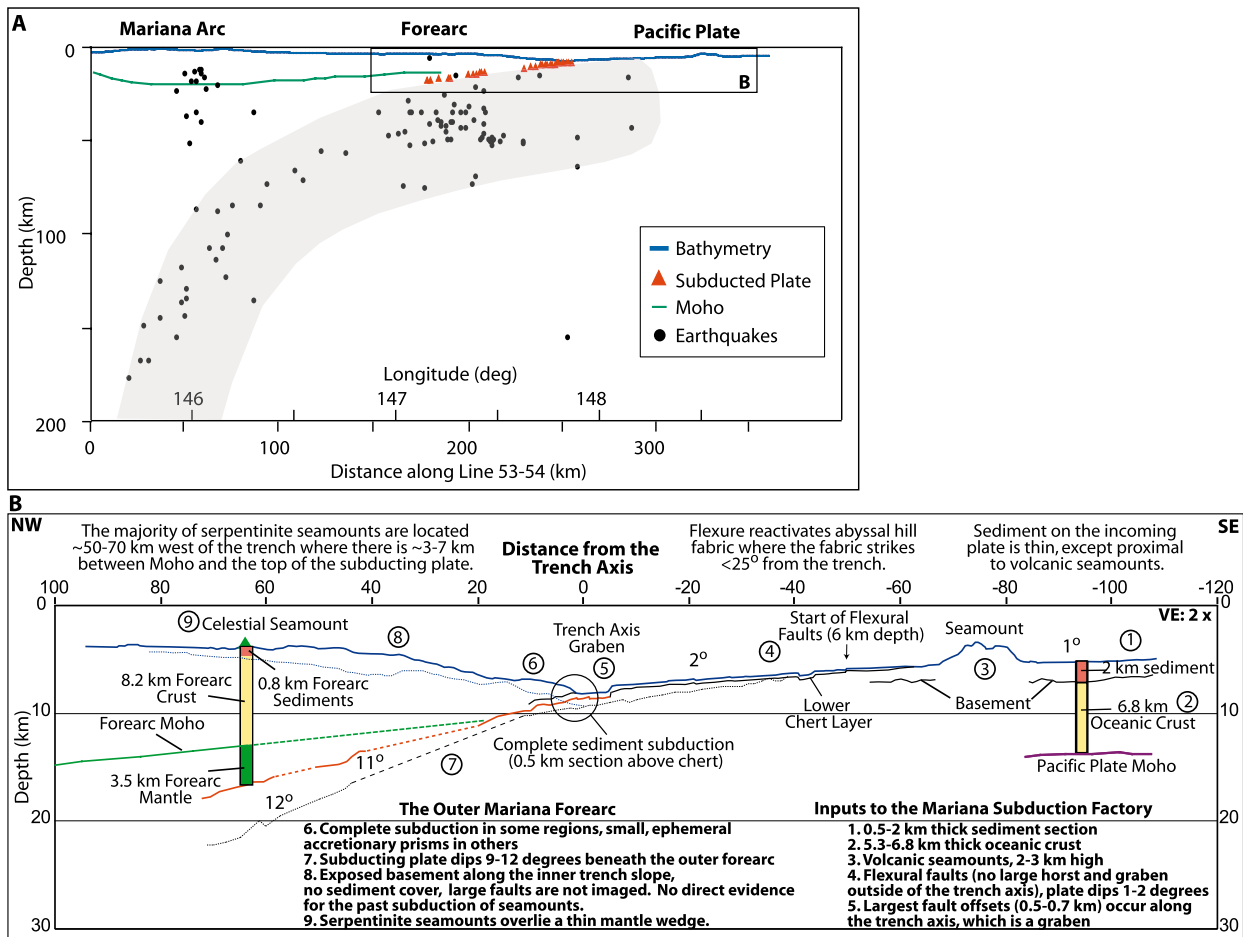
Figure 14. (a) Cross section of the Mariana Subduction System along MCS Line 53–54 with bathymetry (blue), Moho (green) [from *Takahashi et al.*, 2007], top of subducted Pacific Plate (red, this paper), and teleseismic earthquakes recorded within 50 km of the line (black dots) [from *Engdahl et al.*, 1998]. No VE. Inset locates Figure 14b. (b) Enlarged cross section along MCS Line 53–54 of the outer fore arc and subducting plate with numerically annotated features. To illustrate the deeper morphology in Region D, dotted lines show the bathymetry and subducted plate along MCS Line 79–80.

ly, there may be some mantle outcrops along the inner trench slope.

[58] Sedimentation on the outer Mariana fore arc is sparse and therefore we have no seismic resolution to answer the question of underplating versus erosion along the inner trench slope. However, stratigraphic relationships in the inner fore-arc basin indicate that the fore arc in Region D is currently subsiding and tilting toward the trench [*Chapp et al.*, 2005; E. L. Chapp et al., Mariana Forearc basin evolution from 14°N to 18°N: A seismic stratigraphic analysis, submitted to *Geochemistry, Geophysics, Geosystems*, 2008]. This subsidence is relatively recent as evidenced by the onlap of Quaternary sediments onto older, trenchward-tilting, fore-arc basin sediments. The presence of subsidence in the southern fore arc

suggests that there is no significant underplating taking place beneath the outer fore arc. The fore-arc subsidence and trenchward tilting of Region D could result from the removal of material from the underside of the fore arc or the deepening of the subducting plate due to a change in dip.

[59] The presence of the lower slope terrace on the Izu-Bonin fore arc and Region D of the Mariana fore arc is not well understood. There are no obvious faults on Lines Bonin 39, 79–80 or 83–84 that would account for the creation of the lower slope terrace, although a distinct break in slope is visible on the bathymetry (Figures 4 and 8). Our data show that the subducting Pacific Plate is ~2 km deeper in Region D than in Region A, and plate depths beneath the Izu-Bonin fore arc are ~0.5–1.5 km deeper than in Mariana (Figure 12).

In Region D and along the Izu-Bonin margin, the incoming Pacific Plate is deeper, the outer trench slope is steeper and the abyssal hill fabric is parallel to the trench, creating larger offset flexural faults (Figures 4, 8, 13, and 14). The creation of the lower slope terrace and the deepening of the fore arc may be related to the geometry of the plate, specifically its increase in depth on both sides of the trench. The 2 km deepening of the subducted plate in Region D would allow for the subsidence seen in the southern Mariana fore arc basin; however, the plate on Line 79–80 is a kilometer deeper than on 83–84 without a corresponding change in fore-arc bathymetry suggesting that local variations in subducted plate geometry alone may not account for the formation of the entire lower slope terrace and the subsidence.

[60] In Region D, serpentinite velocities (1505 m/s plus a vertical gradient of 1400 m/s/s) were used to depth convert the wedge above the subducting plate reflection, including the possible serpentinite seamount, on Lines 79–80 and 83–84. These velocities successfully corrected for velocity pull-up along the plate reflection, suggesting that much of the lower slope terrace may be composed of serpentinite material.

[61] Previous work inferred that the Mariana fore arc has responded to the collision of oceanic plateaus and seamounts with vertical tectonism [*Fryer and Fryer*, 1987; *Fryer et al.*, 1995], and highs along the trench floor correspond well to highs on the outer fore arc in both Regions A and C (Figure 4). However, although there are numerous normal faults on the fore arc, there is no direct correlation between subducting seamounts and ridges and fore-arc deformation. In fact, in regions like the Celestial Ridge where we might expect to see large faults bounding blocks on the fore arc above a subducting ridge, no faults are visible (Figures 1 and 3). The subducted Pacific Plate is shallowest in Region C beneath Celestial Ridge (Figures 12 and 13). However, there is no apparent onlap or other evidence in the sediments for recent tilting; therefore it is unclear whether or not there is a link between the subducting seamount chain and this outer fore-arc high.

[62] The lack of evidence for disturbance of the upper plate in response to the subduction of seamounts is surprising. The incoming Pacific Plate includes numerous 2–3 km high seamounts and it is reasonable to infer that the Mariana system has been and will continue to be affected by the subduction of these features (Figures 1 and 13). Despite this, we do not see direct bathymetric

evidence in the fore arc (west of the toe of the slope) of the subduction of seamounts. In other regions of the world, subducting seamounts uplift the fore arc and leave large reentrants and grooves in their wake as they plow through the inner trench slope disturbing and removing material (i.e., Nankai Trough, Japan Trench, Costa Rica and Tonga [*Ballance et al.*, 1989; *Yamazaki and Okamura*, 1989; *Dominguez et al.*, 1998; *Ranero and von Huene*, 2000]). *Lallemand and Le Pichon* [1987] show that along the Japan Trench, the subduction of a 1.5 km high seamount caused 1 km of uplift and a 7-km reentrant. Although seamounts of this size are currently subducting in Region A, DSDP Leg 60 scientists found no evidence for kilometric uplift or subsidence at Site 458, southwest of Big Blue Serpentinite Seamount (Figure 1), suggesting long-term stability in this area of the Mariana fore arc [*Hussong and Uyeda*, 1981b].

[63] The Mariana fore arc is home to the only known active serpentinite mud volcanoes in the world [*Fryer and Hussong*, 1981; *Taylor and Smoot*, 1984; *Fryer and Fryer*, 1987; *Horine et al.*, 1990; *Fryer and Mottl*, 1992] and the Mariana margin lacks great earthquakes (M > 8) common in other subduction zones [*Forsyth and Uyeda*, 1975; *Ricard et al.*, 1988; *Huang and Okal*, 1998; *Hyndman and Peacock*, 2003], suggesting that the presence of a serpentinized outer fore arc changes friction properties at the plate boundary. *Hyndman and Peacock* [2003] propose that serpentinite present at the base of the mantle wedge in the fore arc may decrease the coupling between the subducting plate and mantle wedge. The apparent lack of significant deformation of the Mariana fore arc crust by the subduction of large Pacific Plate seamounts may also be the result of a weak serpentinized mantle wedge. In addition, seamounts on the incoming plate are sequentially fractured with increasing offsets as they near the trench axis graben (Figures 5, 6, 7, and 13). The dip of the subducted plate increases by a minimum of 7° within each region of the central Mariana margin as it passes through the trench (Figure 12). This abrupt change in plate dip near the trench axis, along with the degradation of the subducting seamounts, may explain why we do not see significant deformation along the inner trench slope.

5.4. Serpentinite Seamounts, Fore-Arc Mantle, and the Subducting Plate

[64] Serpentinite mud volcanoes form by the eruption of hydrated fore-arc mantle. The degree of

Geochemistry
Geophysics
Geosystems

G^3

OAKLEY ET AL.: PACIFIC PLATE SUBDUCTION

10.1029/2007GC001820

serpentinization of the fore-arc mantle wedge is directly related to the amount of water that chemically interacts with mantle peridotite. Fore-arc mantle lies ~9 km below Celestial Serpentinite Seamount, 64 km from the trench axis [*Takahashi et al.*, 2007]. This region of the fore arc lies at the trench-ward edge of the refraction study and at the edge of good resolution. The Moho inferred from the refraction data is not visible on coincident MCS reflection data. If we run a trend line through Moho depths along the *Takahashi et al.* [2007] refraction line toward the trench, it intersects with the subducting plate ~20–30 km west of the trench at ~11 km depth (Figures 12b and 14). The majority of serpentinite seamounts on the Mariana fore arc are located ~50–70 km west of the trench where there is ~3–7 km of mantle above the subducting plate and below 8–10 km thick fore-arc crust (Figure 12b).

[65] The deep lower slope terrace in Region D may be home to the most trench-proximal serpentinite seamount in the Mariana system, analogous to serpentinite seamounts on the Izu-Bonin fore arc [*Horine et al.*, 1990] (Figures 8 and 12a). The mound imaged on Line 79–80 and in the bathymetry is located approximately 30 km west of the Mariana Trench, near the plate-mantle intersection (Figure 12b). With no samples, nor further constraints on the velocity/density structure, and limited seismic coverage, we cannot be certain that this feature is a serpentinite seamount; however, the presence of serpentinite material in dredges to the north suggests that this is not an unreasonable hypothesis.

6. Summary

[66] On the basis of new MCS and bathymetry data, we created a cross section showing the important features of Pacific Plate subduction beneath the central Mariana fore arc (Figure 14). Our data elucidate important attributes and along-strike variations of the Izu-Bonin-Mariana subduction zone. Oceanic crustal thicknesses along the incoming Pacific Plate are 6 km east of the Izu-Bonin Trench (near ODP Site 1149D) and range from 5.3 to 7 km along the central Mariana margin (14°–19°N). The Pacific oceanic crust is thinly sedimented (0.3–0.5 km) except near seamounts where presumed volcaniclastic sediments increase total thicknesses to 2 km. We observed a seismic reflection near the top of the incoming plate that we correlate with the lower chert layer described in DSDP and ODP drilling results (e.g., Legs 60, 129,

and 185). MCS and swath bathymetry data show that flexure of the incoming plate forms normal faults beginning up to 100 km east of the IBM trench axis. Normal faults that trend obliquely to the Mariana Trench are formed by the reactivation of inherited tectonic fabric striking <25° to the trench. New, trench parallel bending faults are created where the tectonic fabric strikes >25°. Flexural faults along the Izu-Bonin margin are primarily trench-parallel. Bathymetry and MCS profiles show that the incoming plate east of the trench axis is deformed by larger offset horsts and graben in the Izu-Bonin and Tonga subduction zones than in Mariana. The largest fault offsets along the central Mariana margin (0.5–0.7 km) occur along the trench axis, which is commonly a graben. In Mariana a significant change in the dip of the incoming plate from <4° (commonly ≤2°) to >8° occurs within ~10 km of the trench axis. Along the Izu-Bonin and Tonga margins, a similar increase in subducting plate angle occurs ~20 km east of the trench. In all three regions of weak interplate seismic coupling, the abrupt change in dip of the incoming Pacific Plate corresponds to the formation of large offset graben that likely indicate that the plate has failed rather than simply bent. Similar plate kinks beneath the Japan and Hikurangi fore arcs occur seaward of the updip limit of the rupture zones of large earthquakes. The Mariana Trench graben and all the plate kinks are likely the result of slab pull stresses breaking the subducting plate.

[67] In the central Mariana system, seamounts on the subducting Pacific Plate enter the trench axis at 16°N and 18°N and result in the uplift of the toe of the fore arc and shallowing and westward migration of the trench axis. There is evidence from the toe of the inner trench slope for both subduction and small-scale accretion of Pacific Plate sediments along the Mariana Trench. In all regions of the central Mariana margin the lower chert layer and any sediment between chert and basement subduct beyond the outer fore arc. Small accretionary complexes at the toe of the slope are likely to be ephemeral features. We agree with previous work that there has been no long-term sediment accretion in the central Mariana system. The Mariana inner trench slope primarily exposes igneous basement and is covered by discontinuous pockets of thin slope sediments. No large faults were imaged. Unlike other margins subducting large bathymetric highs, west of the toe of the slope we see no direct evidence for disturbance of the upper plate by seamount subduction. This is a

Table A1. Two-Dimensional Processing Sequence (Using ProMAX)

Step	Description
1	Resample to 4 ms.
2	Edit bad traces.
3	Geometry.
4	Sort to Common Mid-Point Gathers (CMP) at 6.25 m.
5	Band-pass filter (4-6-60-70 Hz).
6	Velocity analysis.
7	Normal moveout correction.
8	Top mute.
9	Bottom mute.
10	Pre-stack deconvolution (to remove air gun bubble pulse).
11	Radon velocity filter.
12	CMP ensemble stack.
13	Windowed F−K filter below multiple.
14	Bottom mute just above multiple.
15	Stolt F−K time migration.
16	Automatic Gain Control.
17	Time-varying band-pass filter.
18	Post migration depth conversion.
19	Top mute for display.

surprising conclusion considering the number and size of seamounts visible on the incoming plate and in the trench axis. The apparent lack of significant deformation of the outer Mariana fore arc in response to seamount subduction may be the result of a weak serpentinized mantle wedge and/or progressive fracturing and degradation of the incoming seamounts as the subducting plate breaks and increases in dip as it passes through the trench graben.

[68] There is no evidence for significant underplating of sediments beneath the outer Mariana fore arc. Subsidence in the southern fore arc may reflect basal erosion or an increased depth/dip of the subducted plate. Depths to the top of the subducting plate are deepest along Bonin Line 39 and in Region D of the Mariana fore arc. The formation of the lower slope terrace in these regions may be related to the increased depth of the subducting plate on both sides of the trench. We identified a possible serpentinite seamount on the lower slope terrace in Region D. This seamount, located only 30 km west of the Mariana Trench, may be analogous to serpentinite seamounts on the outer Izu-Bonin fore arc. The MCS data show that the subducting plate dips 9–12 degrees beneath the serpentinite seamounts on the Mariana and Izu-Bonin fore arcs. In Mariana, the majority of the serpentinite seamounts are located ~50–70 km west of the trench

and overlie 8–10 km of fore-arc crust and a thin (3–7 km) mantle wedge.

Appendix A: Methods

[69] The MCS processing sequence applied to all lines is listed in Table A1. We interpret a strong, continuous reflection visible on all of the Mariana MCS lines over the Pacific Plate at ~0.25–0.5 km below seafloor to be correlative with the lower chert layer identified at ODP Site 801 (318–462 mbsf) and use this horizon to indicate the top of the subducting plate. We trace the geophysical contact between the incoming Pacific Plate and the overriding fore arc arcward from the trench. Beneath the outer fore arc we interpret a prominent, normal polarity, low-frequency reflection to be the top of the subducting plate. This reflection is visible on 17 MCS lines; including two from an R/V *Robert Conrad* seismic reflection survey in 1976 (Figure 1). On the final depth converted sections, we picked depths of points along the reflection at the top of the subducting plate (plate-depth picks) beneath the Mariana fore arc with an estimated vertical measurement uncertainty of 1 km (Figure 3). On the basis of our confidence in the plate-depth picks we classified them as A or B. A-picks were reproduced during iterative interpretations by at least two of the authors. B-picks represent areas along the plate reflection where interpretations differed between authors, imaging was low quality, and/or no crosslines were available for comparison. In Figure 12 A-picks are plotted by MCS line number and B-picks from all lines are grouped. Three-dimensional images of the subducted plate surface and contours were created in ArcGIS using a Cokriging method which incorporated satellite gravity data and plate-depths picks (Figure 13). The gravity data were used to constrain variability between the picks and improve the interpolation of the plate surface.

[70] We present bathymetry along existing MCS tracks (labeled by line number) as well as artificially generated profiles (Figures 4 and 8). These profiles are parallel to the track lines and display bathymetry where we have no MCS coverage.

Acknowledgments

References

Abe, K. (1972), Lithospheric normal faulting beneath the Aleutian trench, *Phys. Earth Planet. Inter.*, *5*, 190–198, doi:10.1016/0031-9201(72)90091-X.

Abrams, L. J., R. L. Larson, T. H. Shipley, and Y. Lancelot (1992), The seismic stratigraphy and sedimentary history of the East Mariana and Pigafetta Basins of the western Pacific, *Proc. Ocean Drill. Program Sci. Results*, *129*, 551–569.

Abrams, L. J., R. L. Larson, T. H. Shipley, and Y. Lancelot (1993), Cretaceous volcanic sequences and Jurassic oceanic crust in the East Mariana and Pigafetta basins of the western Pacific, in *The Mesozoic Pacific: Geology, Tectonics, and Volcanism*, *Geophys. Monogr. Ser.*, vol. 77, edited by M. S. Pringle et al., pp. 77–101, AGU, Washington, D. C.

Ammon, C. J., H. Kanamori, and T. Lay (2008), A great earthquake doublet and seismic stress transfer cycle in the central Kuril islands, *Nature*, *451*, 561–564, doi:10.1038/nature06521.

Ballance, P. F., D. V. Scholl, T. L. Vallier, A. J. Stevenson, H. Ryan, and R. H. Herzer (1989), Subduction of the Late Cretaceaous seamount of the Louisville Ridge at the Tonga Trench: A model of normal and accelerated tectonic erosion, *Tectonics*, *8*, 953–962, doi:10.1029/TC008i005p00953.

Billen, M. I., E. Cowgill, and E. Buer (2007), Determination of fault friction from reactivation of abyssal-hill faults in subduction zones, *Geology*, *35*, 819–822, doi:10.1130/G23847A.1.

Bloomer, S. H. (1983), Distribution and origin of igneous rocks from the landward slopes of the Mariana Trench: Implications for its structure and evolution, *J. Geophys. Res.*, *88*, 7411–7428, doi:10.1029/JB088iB09p07411.

Bloomer, S. H., and J. W. Hawkins (1983), Gabbroic and ultramafic rocks from the Mariana trench: An island arc ophiolite, in *The Tectonic and Geologic Evolution of the Southeast Asian Seas and Islands: Part 2*, *Geophys. Monogr. Ser.*, vol. 27, edited by D. E. Hayes, pp. 294–317, AGU, Washington, D. C.

Bodine, J. H., and A. B. Watts (1979), On lithospheric flexure seaward of the Bonin and Mariana trenches, *Earth Planet. Sci. Lett.*, *43*, 132–148, doi:10.1016/0012-821X(79)90162-6.

Chapp, E. L., B. Taylor, A. J. Oakley, and G. Moore (2005), Seismic stratigraphy of the Mariana forearc sedimentary basin, *Eos Trans. AGU*, *86*(52), Fall Meet. Suppl., Abstract T53A-1403.

Chiu, J. M., B. L. Isacks, and R. K. Cardwell (1991), 3-D configuration of subducted lithosphere in the western Pacific, *Geophys. J. Int.*, *106*, 99–111, doi:10.1111/j.1365-246X.1991.tb04604.x.

Clift, P., and P. Vannucchi (2004), Controls on tectonic accretion versus erosion in subduction zones: Implications for the origin and recycling of the continental crust, *Rev. Geophys.*, *42*, RG2001, doi:10.1029/2003RG000127.

Cosca, M. A., R. J. Arculus, J. A. Pearce, and J. G. Mitchell (1998), $^{40}Ar/^{39}Ar$ and K-Ar age constraints for the inception and early evolution of the Izu-Bonin-Mariana arc system, *Island Arc*, *7*, 579–595, doi:10.1111/j.1440-1738.1998.00211.x.

Dominguez, S., S. E. Lallemand, J. Malavieille, and R. von Huene (1998), Upper plate deformation associated with seamount subduction, *Tectonophysics*, *293*, 207–224, doi:10.1016/S0040-1951(98)00086-9.

Dominguez, S., J. Malavieille, and S. E. Lallemand (2000), Deformation of accretionary wedges in response to seamount subduction: Insights from sandbox experiments, *Tectonics*, *19*, 182–196, doi:10.1029/1999TC900055.

Eiler, J. (Ed.) (2003), *Inside the Subduction Factory*, *Geophys. Monogr. Ser*, vol. 138, AGU, Washington, D. C.

Elliott, T., T. Plank, A. Zindler, W. White, and B. Bourdon (1997), Element transfer from slab to volcanic front at the Mariana arc, *J. Geophys. Res.*, *102*, 14,991–15,019, doi:10.1029/97JB00788.

Engdahl, E. R., R. D. van der Hilst, and R. P. Buland (1998), Global teleseismic earthquake relocation with improved travel times and procedures for depth determination, *Bull. Seismol. Soc. Am.*, *88*, 722–743.

Ewing, J., M. Ewing, T. Altken, and W. J. Ludwig (1968), North Pacific sediment layers measured by seismic profiling, in *The Crust and Upper Mantle of the Pacific Area*, *Geophys. Monogr. Ser*, vol. 12, edited by L. Knopoff et al., pp. 147–173, AGU, Washington, D. C.

Forsyth, D. W., and S. Uyeda (1975), On the relative importance of the driving forces of plate motion, *Geophys. J.*, *43*, 163–200.

Fryer, P., and G. J. Fryer (1987), Origins of nonvolcanic seamounts in a forearc environment, in *Seamounts, Islands and Atolls*, edited by B. Keating et al., pp. 61–69, *Geophys. Monogr. Ser.*, vol. 43, AGU, Washington, D. C.

Fryer, P., and D. M. Hussong (1981), Seafloor spreading in the Mariana Trough: Results of Leg 60 drill site selection surveys, *Initial Rep. Deep Sea Drill. Proj.*, *60*, 45–55.

Fryer, P., and M. Mottl (1992), Lithology, mineralogy, and origin of serpentine muds recovered from Conical and Torishima forearc seamounts: Results of Leg 125 drilling, *Proc. Ocean Drill. Program Sci. Results*, *125*, 343–362.

Fryer, P., E. L. Ambos, and D. M. Hussong (1985), Origin and emplacement of Mariana forearc seamounts, *Geology*, *13*, 774–777, doi:10.1130/0091-7613(1985)13<774:OAEOMF>2.0.CO;2.

Fryer, P., M. Mottl, L. Johnson, J. A. Haggerty, S. Phipps, and H. Maekawa (1995), Serpentine bodies in the forearcs of western Pacific convergent margins: Origin and associated fluids, in *Active Margins and Marginal Basins of the Western Pacific*, *Geophys. Monogr. Ser*, vol. 88, edited by B. Taylor and J. Natland, pp. 259–279, AGU, Washington, D. C.

Fryer, P., J. P. Lockwood, N. Becker, S. Phipps, and C. S. Todd (2000), Significance of serpentine mud volcanism in convergent margins, *Spec. Pap. Geol. Soc. Am.*, *349*, 35–51.

Fujie, G., A. Ito, S. Kodaira, N. Takahashi, and Y. Kaneda (2006), Confirming sharp bending of the Pacific plate in the northern Japan trench subduction zone by applying a traveltime mapping method, *Phys. Earth Planet. Inter.*, *157*, 72–85, doi:10.1016/j.pepi.2006.03.013.

Gharib, J. (2006), Clastic metabasites and authigenic minerals within serpentinite protrusions from the Mariana Forearc: Implications for sub-forearc subduction processes, Ph.D. thesis, 239 pp., Univ. of Hawaii, Honolulu.

Haggerty, J. A. (1987), Petrology and geochemistry of Neogene sedimentary rocks from Mariana forearc seamounts: Implications for emplacement of the seamounts, *Seamounts, Islands and Atolls*, edited by B. Keating et al., pp. 175–185, *Geophys. Monogr. Ser.*, vol. 43, AGU, Washington, D. C.

Henrys, S., M. Reyners, I. Pecher, S. Bannister, Y. Nishimura, and G. Maslen (2006), Kinking of the subducting slab by

escalator normal faulting beneath the North Island of New Zealand, *Geology*, *34*, 777–780, doi:10.1130/G22594.1.

Horine, R. L., G. F. Moore, and B. Taylor (Eds.) (1990), *Structure of the Outer Izu-Bonin Forearc From Seismic-Reflection Profiling and Gravity Modeling*, U. S. Govt. Print. Off., Washington, D. C.

Huang, W.-C., and E. Okal (1998), Centroid-moment-tensor solutions for deep earthquakes predating the digital era: Discussion and inferences, *Phys. Earth Planet. Inter.*, *106*, 191–218, doi:10.1016/S0031-9201(97)00111-8.

Hussong, D. M., and P. Fryer (1981), Structure and tectonics of the Mariana Arc and Forearc: Drillsite selection surveys, *Initial Rep. Deep Sea Drill. Proj.*, *60*, 33–44.

Hussong, D. M., and S. Uyeda (Eds.) (1981a), *Initial Reports of the Deep Sea Drilling Project*, Leg 60, U. S. Govt. Print. Off., Washington, D. C.

Hussong, D. M., and S. Uyeda (1981b), Tectonic processes and the history of the Mariana arc: A synthesis of the results of Deep Sea Drilling Project Leg 60, *Initial Rep. Deep Sea Drill. Proj.*, *60*, 909–929.

Hyndman, R. D., and S. M. Peacock (2003), Serpentinization of the forearc mantle, *Earth Planet. Sci. Lett.*, *212*, 417–432, doi:10.1016/S0012-821X(03)00263-2.

Isacks, B. L., and M. Barazangi (1977), Geometry of Benioff Zones: Lateral segmentation and downwards bending of the subducted lithosphere, in *Island Arcs, Deep Sea Trenches, and Back-Arc Basins*, *Maurice Ewing Ser.*, vol. 1, edited by M. Talwani and W. C. Pitman, pp. 99–114, AGU, Washington, D. C.

Ito, A., G. Fujie, T. Tsuru, S. Kodaira, A. Nakanishi, and Y. Kaneda (2004), Fault plane geometry in the source region of the 1994 Sanriku-oki earthquake, *Earth Planet. Sci. Lett.*, *223*, 163–175, doi:10.1016/j.epsl.2004.04.007.

Ito, A., G. Fujie, S. Miura, S. Kodaira, and Y. Kaneda (2005), Bending of the subducting oceanic plate and its implication for rupture propagation of large interplate earthquakes off Miyagi, Japan, in the Japan Trench subduction zone, *Geophys. Res. Lett.*, *32*, L05310, doi:10.1029/2004GL022307.

Kamimura, A., J. Kasahara, M. Shinohara, R. Hino, H. Shiobara, G. Fujie, and T. Kanazawa (2002), Crustal structure study at the Izu-Bonin subduction zone around 31N: Implications of serpentinitized materials along the subduction boundary, *Phys. Earth Planet. Inter.*, *132*, 105–129, doi:10.1016/S0031-9201(02)00047-X.

Kanamori, H. (1971), Seismological evidence for a lithospheric normal faulting: The Sanriku earthquake of 1933, *Phys. Earth Planet. Inter.*, *4*, 289–300, doi:10.1016/0031-9201(71)90013-6.

Kanamori, H. (1986), Rupture process of subduction zone earthquakes, *Annu. Rev. Earth Planet. Sci.*, *14*, 293–322, doi:10.1146/annurev.ea.14.050186.001453.

Karig, D. E. (1971a), Origin and development of marginal basins in the western Pacific, *J. Geophys. Res.*, *76*, 2542–2561, doi:10.1029/JB076i011p02542.

Karig, D. E. (1971b), Structural history of the Mariana island arc system, *Geol. Soc. Am. Bull.*, *82*, 323–344, doi:10.1130/0016-7606(1971)82[323:SHOTMI]2.0.CO;2.

Karig, D. E., and B. Ranken (1983), Marine geology of the forearc region, southern Mariana island arc, in *The Tectonic and Geologic Evolution of the Southeast Asian Seas and Islands: Part 2*, *Geophys. Monogr. Ser.*, vol. 27, edited by D. E. Hayes, pp. 266–280, AGU, Washington, D. C.

Katsumata, M., and L. Sykes (1969), Seismicity and tectonics of the western Pacific: Izu-Mariana-Caroline and Ryukyu-Taiwan regions, *J. Geophys. Res.*, *74*, 5923–5948, doi:10.1029/JB074i025p05923.

Lallemand, S. E., and X. Le Pichon (1987), Coulomb wedge model applied to the subduction of seamounts in the Japan Trench, *Geology*, *15*, 1065–1069, doi:10.1130/0091-7613(1987)15<1065:CWMATT>2.0.CO;2.

Lallemand, S. E., R. Culotta, and R. von Huene (1989), Subduction of the Daiichi Kashima Seamount in the Japan Trench, *Tectonophysics*, *160*, 231–247, doi:10.1016/0040-1951(89)90393-4.

Lallemand, S. E., P. Schnurle, and J. Malavieille (1994), Coulomb theory applied to accretionary and nonaccretionary wedges: Possible causes for tectonic erosion and/or frontal accretion, *J. Geophys. Res.*, *99*, 12,033–12,055, doi:10.1029/94JB00124.

LaTraille, S. L., and D. M. Hussong (1980), Crustal structure across the Mariana island arc, in *The Tectonic and Geologic Evolution of Southeast Asian Seas and Islands*, *Geophys. Monogr. Ser.*, vol. 23, edited by D. E. Hayes, pp. 209–221, AGU, Washington, D. C.

Lonsdale, P. (1986), A multibeam reconnaissance of the Tonga Trench axis and its intersection with the Loisville Guyot chain, *Mar. Geophys. Res.*, *8*, 295–327, doi:10.1007/BF02084016.

Maekawa, H., P. Fryer, and A. Ozaki (1995), Incipient blueschist-facies metamorphism in the active subduction zone beneath the Mariana forearc, in *Active Margins and Marginal Basins of the Western Pacific*, *Geophys. Monogr. Ser.*, vol. 88, edited by B. Taylor and J. Natland, pp. 281–289, AGU, Washington, D. C.

Mottl, M. (1992), Pore waters from serpentinite seamounts in the Mariana and Izu-Bonin forearcs, Leg 125: Evidence for volatiles from the subducting slab, *Proc. Ocean Drill. Program Sci. Results*, *125*, 373–385.

Mottl, M. J., S. C. Komor, P. Fryer, and C. L. Moyer (2003), Deep-slab fluids fuel extremophilic Archaea on a Mariana forearc serpentinite mud volcano: Ocean Drilling Program Leg 195, *Geochem. Geophys. Geosyst.*, *4*(11), 9009, doi:10.1029/2003GC000588.

Mottl, M., C. G. Wheat, P. Fryer, and J. Gharib (2004), Chemistry of springs across the Mariana forearc shows progressive devolatilization of the subducting plate, *Geochim. Cosmochim. Acta*, *68*, 4915–4933, doi:10.1016/j.gca.2004.05.037.

Mrozowski, C. L., D. E. Hayes, and B. Taylor (1981), Multichannel seismic reflection surveys of Leg 60 sites, Deep Sea Drilling Project, in *Initial Rep. Deep Sea Drill. Proj.*, *60*, 57–69.

Nakanishi, M., K. Tamaki, and K. Kobayashi (1992a), Magnetic anomaly lineations from Late Jurassic to Early Cretaceous in the west-central Pacific Ocean, *Geophys. J. Int.*, *109*, 701–719, doi:10.1111/j.1365-246X.1992.tb00126.x.

Nakanishi, M., K. Tamaki, and K. Kobayashi (1992b), A new Mesozoic isochron chart of the northwestern Pacific Ocean: Paleomagnetic and tectonic implications, *Geophys. Res. Lett.*, *19*, 693–696, doi:10.1029/92GL00022.

Oakley, A. J., B. Taylor, P. Fryer, G. Moore, A. Goodliffe, and J. K. Morgan (2007), Emplacement, growth and gravitational deformation of serpentinite seamounts on the Mariana forearc, *Geophys. J. Int.*, *170*, 615–634, doi:10.1111/j.1365-246X.2007.03451.x.

Peacock, S. M. (1990), Fluid Processes in subduction zones, *Science*, *248*, 329–337, doi:10.1126/science.248.4953.329.

Plank, T., and C. H. Langmuir (1993), Tracing trace elements from sediment input to volcanic output at subduction zones, *Nature*, *362*, 739–743, doi:10.1038/362739a0.

Ranero, C. R., and V. Sallares (2004), Geophysical evidence for hydration of the crust and mantle of the Nazca plate

during bending at the north Chile trench, *Geology*, *32*, 549–552, doi:10.1130/G20379.1.

Ranero, C. R., and R. von Huene (2000), Subduction erosion along the Middle America convergent margin, *Nature*, *404*, 748–752, doi:10.1038/35008046.

Ranero, C. R., J. Phipps Morgan, K. McIntosh, and C. Reichert (2003), Bending-related faulting and mantle serpentinization at the Middle America trench, *Nature*, *425*, 367–373, doi:10.1038/nature01961.

Ricard, Y., C. Froidevaux, and L. Fleitout (1988), Global plate motion and the geoid: A physical model, *Geophys. J.*, *93*, 477–484.

Savov, I. P., J. G. Ryan, M. D'Antonio, and P. Fryer (2007), Shallow slab fluid release across and along the Mariana arc-basin system: Insights from geochemistry of serpentinized peridotites from the Mariana fore arc, *J. Geophys. Res.*, *112*, B09205, doi:10.1029/2006JB004749.

Schmidt, M. W., and S. Poli (1998), Experimentally based water budgets for dehydrating slabs and consequences for arc magma generation, *Earth Planet. Sci. Lett.*, *163*, 361–379, doi:10.1016/S0012-821X(98)00142-3.

Shipboard Scientific Party (1990), Leg 129 explanatory notes, *Proc. Ocean Drill. Program Initial Rep.*, *129*, 5–29.

Shipboard Scientific Party (2000), Leg 185 summary: Inputs to the Izu-Mariana subduction system, *Proc. Ocean Drill. Program Initial Rep.*, *185*, 1–63.

Stern, R., M. J. Fouch, and S. L. Klemperer (2003), An overview of the Izu-Bonin-Mariana Subduction Factory, in *Inside the Subduction Factory*, *Geophys. Monogr. Ser.*, vol. 138, edited by J. Eiler, pp. 175–222, AGU, Washington, D. C.

Straub, S. M., and G. D. Layne (2003), Decoupling of fluids and fluid-mobile elements during shallow subduction: Evidence from halogen-rich andesite melt inclusions from the Izu arc volcanic front, *Geochem. Geophys. Geosyst.*, *4*(7), 9004, doi:10.1029/2002GC000349.

Takahashi, N., S. Kodaira, S. L. Klemperer, Y. Tatsumi, Y. Kaneda, and K. Suyehiro (2007), Crustal structure and evolution of the Mariana intra-oceanic island arc, *Geology*, *35*, 203–206, doi:10.1130/G23212A.1.

Taylor, B. (1992), Rifting and the volcanic-tectonic evolution of the Izu-Bonin-Mariana arc, *Proc. Ocean Drill. Program Sci. Results*, *126*, 627–651.

Taylor, B., and N. C. Smoot (1984), Morphology of Bonin fore-arc submarine canyons, *Geology*, *12*, 724–727, doi:10.1130/0091-7613(1984)12<724:MOBFSC>2.0.CO;2.

Ulmer, P., and V. Trommsdorff (1995), Serpentine stability to mantle depths and subduction-related magmatism, *Science*, *268*, 858–861, doi:10.1126/science.268.5212.858.

Uyeda, S. (1982), Subduction zones (introduction to comparative subductology), *Tectonophysics*, *81*, 133–159, doi:10.1016/0040-1951(82)90126-3.

von Huene, R., and R. Culotta (1989), Tectonic erosion at the front of the Japan Trench convergent margin, *Tectonophysics*, *160*, 75–90, doi:10.1016/0040-1951(89)90385-5.

von Huene, R., and D. W. Scholl (1991), Observations at convergent margins concerning sediment subduction, subduction erosion, and the growth of continental crust, *Rev. Geophys.*, *29*, 279–316, doi:10.1029/91RG00969.

Wessel, P. (2001), Global distribution of seamounts inferred from gridded Geostat/ERS-1 altimetry, *J. Geophys. Res.*, *106*, 19,431–19,441, doi:10.1029/2000JB000083.

Yamazaki, T., and Y. Okamura (1989), Subducting seamounts and deformation of overriding forearc wedges around Japan, *Tectonophysics*, *160*, 207–229, doi:10.1016/0040-1951(89)90392-2.